

# Inter-basin versus intra-basin sea surface temperature forcing of the Western North Pacific subtropical high's westward extensions

**Jhordanne J. Jones<sup>1,2\*</sup>, Daniel R. Chavas<sup>2</sup>, Zachary F. Johnson<sup>3</sup>**

<sup>1</sup>University Corporation for Atmospheric Research, Boulder, CO, USA

<sup>2</sup>Department of Earth, Atmospheric, and Planetary Sciences, Purdue University, West Lafayette, IN, USA  
<sup>3</sup>Department of Earth and Atmospheric Sciences, Central Michigan University, Mount Pleasant, MI, USA

<sup>3</sup>Department of Earth and Atmospheric Science, Central Michigan University, Mount Pleasant, MI, USA

## **Key Points:**

- Two similar SST patterns belie two different mechanisms forcing the subtropical high's westward extensions.
  - Tropical Pacific SST gradient forcing of westward extensions can be suppressed by its extra-tropical SST forcing.
  - Remote Atlantic SST forcing drives westward extensions when the local net Pacific forcing is weak.

---

<sup>\*</sup>Department of Earth, Atmospheric, and Planetary Science, Purdue University

Corresponding author: Dr. Jhordanne Jones, jjpjones@purdue.edu

**Abstract**

Zonal extensions of the Western Pacific subtropical high (WPSH) strongly modulate extreme rainfall activity and tropical cyclone (TC) landfall over the Western North Pacific (WNP) region. On seasonal timescales, these zonal extensions are forced primarily by inter-basin zonal sea surface temperature (SST) gradients. However, despite the presence of large-scale zonal SST gradients, the WPSH's response to SSTs varies from year to year. In this study, we force the atmosphere-only NCAR Community Earth System Model version 2 simulations with two real-world SST patterns, both featuring the large-scale zonal SST gradient characteristic of decaying El Niño/developing La Niña summers. For each of these patterns, we perform four experimental sets that test the relative contributions of the tropical Indian Ocean, Pacific, and Atlantic basin SSTs to simulated westward extensions over the WNP during June-August. Our results indicate that the subtle differences between the two SST anomaly patterns belie two different mechanisms forcing the WPSH's westward extensions. In one SST pattern, the extratropical North Pacific SST forcing suppresses the tropical Pacific zonal SST gradient forcing, resulting in tropical Atlantic and Indian Ocean SST warming being the main drivers of the Walker Circulation. With an adjacent SST pattern, subsidence over the WNP is driven predominantly by intra-basin Pacific SST forcing. The results of this study have implications for understanding and predicting the impact of the WPSH's zonal variability on tropical cyclones and extreme rainfall over the WNP.

**Plain Language Summary**

Westward extensions of the Western North Pacific subtropical high (WPSH) drive rainfall extremes over the Western North Pacific basin, and is important for the prediction of summer rainfall, including monsoonal rainfall and tropical cyclone activity. Studies have previously highlighted the importance of the large-scale zonal sea surface temperature (SST) gradient - warm tropical Indian Ocean in conjunction with cold equatorial eastern Pacific Ocean - in developing and maintaining the summer WPSH and westward extensions. But, here, we show that even with very similar SST patterns, the large-scale zonal SST pattern may belie forcing from inter-basin SSTs versus intra-basin SSTs. We find that the degree of spread of negative SST anomalies across the central and eastern Pacific region may determine whether inter-basin versus intra-basin Pacific SSTs are the predominant driver of westward extensions.

**1 Introduction**

The Western Pacific subtropical high (WPSH) is an important driver of weather and climate variability over the Western North Pacific (WNP) region. The WPSH's variability is key in the prediction of boreal summer rainfall variability across the Indo-Pacific region, including East Asian monsoon rainfall (B. Wang et al., 2013; Guan et al., 2019), Indian summer rainfall (Chaluvadi et

al., 2021), and tropical cyclone (TC) activity (B. Wang et al., 2013; Camp et al., 2018; Q. Wu et al., 2020; Johnson et al., 2022). Chang et al. (2000) observed that a westward extension of the WPSH's western edge is associated with increased monsoonal rainfall over East Asia, as an anomalous low-level westerly circulation channels moisture into the Yangtze River basin. B. Wang et al. (2013) showed that WPSH variability afforded considerable skill to WNP TC predictability, while Camp et al. (2018) demonstrated that TC predictability in models was strong due to a well-simulated WPSH. Studies such as Johnson et al. (2022) further showed that the WPSH's zonal variations or extensions play a substantial role in influencing seasonal WNP TC landfalling events.

Zonal extensions of the WPSH are characterized by anomalous geopotential heights over the WNP, along the WPSH's western edge, and strong easterly flow along the southern edge. Their interannual variability is strongly influenced by both local and remote sea surface temperature (SST) forcing (Lu, 2001; Lu & Dong, 2001; Dong et al., 2017; Guan et al., 2019). Known local SST forcings include the Pacific warm pool region (Lu, 2001; Lu & Dong, 2001), while the tropical Indian Ocean (TIO) (Xie et al., 2009, 2016; Kosaka et al., 2013; He & Zhou, 2015; Qian & Shi, 2017), the central (CP) and eastern Pacific (EP) regions (B. Wu et al., 2010; B. Wang et al., 2013; H. Li et al., 2020) have been identified as key remote forcings of WPSH variability. Alternatively, North Atlantic (ATL) SST variability may play a remote role in intensifying the WPSH and forcing WPSH meridional extensions (T. Li et al., 2017; Feng & Chen, 2021). The differential diabatic heating related to monsoons and the land-sea contrast is also important (Rodwell & Hoskins, 2001; Liu et al., 2004). Seager et al. (2003) suggested that the air-sea interaction and SST asymmetry amplify the circulation responses to monsoonal forcing. Furthermore, they showed that the global subtropical highs (STHs) reach their peak in the summer due to the strengthening of the west-east positive-negative SST asymmetry across each basin. Both B. Wang et al. (2013) and Kosaka et al. (2013) later showed that the leading modes of WPSH variability were supported by distinct modes of underlying zonal SST gradients.

A number of studies have shown that the WPSH has diverse responses to varying regional SST forcing within the underlying large-scale SST pattern. Many have shown that colder equatorial CP and EP SSTs enhance the WPSH and thus promote a stronger westward extension (B. Wu et al., 2010; Yuan & Yan, 2013; Z. Chen et al., 2016, 2017; M. Chen et al., 2019). M. Chen et al. (2019) found that differences in the preceding year's El Niño warming pattern resulted in varying WPSH development and intensification by different mechanisms. Jong et al. (2020) showed that summers with a transitional La Niña produced a stronger WNP anticyclone than La Niña-persisting summers. More recently, (Jiang et al., 2023) examined the diversity in WPSH response among seasons characterized by fast-decay El Niño events and showed that the WPSH's westward extensions were sensitive to SST differences. Faster El Niño decay rates resulted in the La Niña cold tongue reaching longitudes east of 160°E during June-August. The La Niña's cold anomalies promoted

85 subsidence over the WNP and anomalous anticyclonic flow. Slower decay rates resulted in lingering  
86 El Niño-associated warming that promoted convection and cyclonic flow over the WNP.

87 Atlantic (ATL) warming also plays a role in the WPSH's varying response during La Niña-  
88 developing summers (Hong et al., 2014, 2015; Zuo et al., 2019; Feng et al., 2020; Feng & Chen,  
89 2021). But, many of the aforementioned studies have assessed the relative contributions of local and  
90 remote SST forcing to differences in WPSH response. Very few have examined the relative roles of  
91 tropical Indian Ocean, Pacific and Atlantic SST forcing in SST patterns that produce very similar  
92 responses in the WPSH. B. Wang et al. (2013) earlier demonstrated that the first two leading modes  
93 of WPSH variability, producing similar WPSH intensity, were driven by different atmosphere-ocean  
94 mechanisms. The first leading mode was characterized by a tropical Indian Ocean-WNP inter-basin  
95 zonal SST gradient. The second leading mode was characterized by an intra-basin warm WNP-cool  
96 CP and EP. In this study, we explore the relative contribution of regional SST forcing by comparing  
97 two large-scale SST patterns that produce very similar WPSH response. Here, we define inter-basin  
98 forcing as the remote impact of an external ocean to the atmospheric climate over the Pacific basin,  
99 while we use the term intra-basin to describe the impact of the local Pacific SSTs on the Pacific  
100 atmosphere.

101 While some of our conclusions are very similar to Jiang et al. (2023). We additionally show  
102 that similar changes in El Niño decay rate can also assess whether the underlying mechanism is  
103 inter-basin or intra-basin in nature. We explore the characteristic SST gradient pattern associated  
104 with the WPSH's westward extensions and compare the contribution of both inter-basin and intra-  
105 basin SST forcings to the WPSH's zonal variability. We compare whether the WPSH extensions  
106 are responding to single-region anomaly SST forcings (e.g. TIO and ATL SSTs) or SST gradient  
107 forcings. Additionally, we compare two similar large-scale SST patterns and assess how and why  
108 they provoke different atmospheric responses over the WNP, and assess the contributions from both  
109 local and remote SST forcings in each case. The questions we address in this paper are outlined as  
110 follows:

- 111 1. Can a comparable westward extension of the STH be forced by inter-basin and intra-basin  
112 SST drivers?
- 113 2. Which regional SST differences promote an inter-basin versus intra-basin mechanism?
- 114 3. How do the roles of the tropical Indian Ocean SSTs, equatorial central and eastern Pacific  
115 SSTs, and North Atlantic Ocean SSTs vary in an inter-basin versus intra-basin SST forcing?

116 The paper is outlined as follows. In section 2, we describe the data, methods, and experimental  
117 setup. Section 3 provides an observational analysis of the two similar SST patterns and their im-  
118 pact on the WPSH and its westward extensions. Section 4 outlines the results of our SST forcing  
119 experiments. Section 5 gives the discussion and conclusions.

120 **2 Data and Methods**121 **2.1 Data**

122 Monthly variable fields are sourced from the ECMWF fifth generation reanalysis (ERA5)  
 123 dataset (Hersbach et al., 2020). The ERA5 reanalysis dataset has a horizontal grid resolution  
 124 of 31 km with 137 vertical levels, and provides data from 1 January 1940 to the present. Vari-  
 125 ables with a  $0.25^\circ \times 0.25^\circ$  grid resolution were obtained from the Copernicus Climate Data Store  
 126 (<https://cds.climate.copernicus.eu/cdsapp#!/home>) and are as follows: 850-  
 127 hPa geopotential heights (Z850), 250-hPa, and 850-hPa zonal and meridional winds (UV250,  
 128 UV850), and sea surface temperatures (SSTs). We analyze these fields over the time period 1979-  
 129 2019. Anomalies calculated from these fields are relative to the 1979-2019 mean climatology. Note  
 130 that our anomaly fields have not been detrended. In Section 3, we use the reanalysis variable fields  
 131 to examine and characterize anomaly composites associated with the WPSH's extensions.

132 The WPSH's intensity and westward extensions are determined using the Z850 anomaly field.  
 133 There are a variety of ways in which WPSH variability may be defined. Common indices used  
 134 are calculated with geopotential height anomalies at 850-hPa (B. Wang et al., 2013; Camp et al.,  
 135 2018) and 500-hPa (Zhou et al., 2009; Qian & Shi, 2017; H. Li et al., 2020). Less commonly used  
 136 indices include 850-hPa relative vorticity (Kosaka et al., 2013; X. Wang et al., 2021). Following  
 137 B. Wang et al. (2013), Camp et al. (2018), and Johnson et al. (2022), we define the WPSH intensity  
 138 using 850-hPa geopotential height anomalies averaged over the tropical WNP region ( $10^\circ\text{-}30^\circ\text{N}$ ,  
 139  $100^\circ\text{E}\text{-}180^\circ$ ). We also define the westward extension index (WEI) as the most westward longitude  
 140 reached along the 1510-m contour within the WNP region. Under warming, positive geopotential  
 141 height anomalies spread across the WNP due to atmospheric expansion, giving the illusion that the  
 142 Pacific STH extends westward when measured by the spatial extent of a given height. Dong and He  
 143 (2020) and H. Li et al. (2020) use similar methods to characterize the WPSH's zonal extensions in  
 144 the 500-hPa height fields. The SST fields are used to calculate monthly standardized anomalies for  
 145 the tropical Indian Ocean (TIO,  $30^\circ\text{S}\text{-}30^\circ\text{N}$ ,  $40^\circ\text{-}120^\circ\text{E}$ ), WNP, tropical North Atlantic ( $0^\circ\text{-}20^\circ\text{N}$ ,  
 146  $100^\circ\text{W}\text{-}0^\circ$ ) and El Niño Southern Oscillation (ENSO) SST variability. The conventional Niño-3.4  
 147 region has been extended to  $160^\circ\text{E}$  to better capture non-linear seasonal cold-tongue SST variations  
 148 in the Central Pacific and equatorial eastern Pacific, as proposed by Williams and Patricola (2018).  
 149 Therefore, the acronym ENSO is used hereafter to refer to the deep tropical equatorial Pacific SST  
 150 anomalies between  $10^\circ\text{S}\text{-}10^\circ\text{N}$  and  $160^\circ\text{E}\text{-}120^\circ\text{W}$ .

151 **2.2 CAM6 and Experiment Setup**

152 We simulate the response of the WPSH using the atmosphere-only component of Commu-  
 153 nity Earth System Model version 2.2.0 (CESM2). The Community Atmosphere Model version

154       6 (CAM6) uses a  $0.9^\circ \times 1.25^\circ$  horizontal resolution and 32 vertical levels with a Finite Volume  
155       (FV) dynamical core (Danabasoglu et al., 2020). Our experimental setup consists of atmosphere-only  
156       (AMIP) simulations using the F2000CLIMO configuration driven by a historical 12-monthly  
157       SST climatology representative of present-day climate, and is run with active atmosphere (CAM6)  
158       and land (CLM5) components. A detailed description of F2000CLIMO and other CESM2 run  
159       configurations can be found at <https://www.cesm.ucar.edu/models/cesm2/config/compsets.html>. The F2000CLIMO compset provides a simplified experimental setup that di-  
160       rectly tests the general circulation's response to recurring seasonal SST changes independent of  
161       year-to-year SST variability.

163       To examine how SSTs force the WPSH, we run the F2000CLIMO component set that forces  
164       CAM6 with a 12-month prescribed SST climatology. The control experiment (CTRL) is taken to  
165       be the 1979-2019, calculated from the ERA5 reanalysis dataset. Note that the ERA5 SST fields are  
166       regridded to the CAM6 grid resolution ( $1.9^\circ \times 2.5^\circ$ ), and are linearly interpolated to fill in masked  
167       land values prior to running the simulations. The first SST composite (COMP1) comprise years  
168       1980, 1995, 1998, 2003, and 2010, in which the June-August WPSH is most enhanced and the  
169       1510-gph contour is most westward extended. The second SST forcing (COMP2) is composited  
170       from years 1980, 1983, 1998, 1999, and 2010. While there is considerable overlap between the  
171       two sets of years, the addition of 1983 and 1999 in COMP2 results in a larger spread of negative  
172       SST anomalies across the central and eastern Pacific regions without significantly changing the  
173       magnitude of the La Niña (Figure 2). This partial overlap is by design. As we will show below,  
174       somewhat subtle differences in SST anomaly patterns between the two composites result in markedly  
175       different outcomes for the drivers of the westward extension. In practice, experiments for these two  
176       distinct composites were initially done by accident, but serendipitously, they yielded an interesting  
177       contrast in behavior that became the focus of this work. Then, the COMP1 and COMP2 SST patterns  
178       are quadrupled in magnitude ( $4xWEST$ ) to enhance the westward extension signal in the simulations  
179       relative to the CTRL simulation. The simulations are allowed to run for 6 years. The first year is  
180       thrown out to account for model initialization, and the atmospheric response is averaged over years  
181       2-6. We ran initial experiments out to years 6, 11, 16, and 31 and found no significant changes from  
182       the simulated westward extent averaged over years 2-6.

183       Note that, since the simulations are driven only by the prescribed 12-month SST climatology,  
184       the simulations are not forced by SST variations from preceding years, and therefore, doesn't take  
185       into account lagged air-ocean impacts, for example, ENSO's and TIO's lagged relationships from the  
186       year prior (M. Chen et al., 2019). Similarly, the WPSH is also a result of coupled air-sea interactions  
187       (T. Li et al., 2017). The study to follow only examines the atmospheric response to the prescribed  
188       SSTs. In the sections to follow, we compare the WPSH's response across the  $4xWEST$  simulations.

189 To test which specific regional SST anomalies generate an enhanced WPSH comparable to  
 190 the original *4xWEST* simulations, we run a set of experiments in which we progressively constrain  
 191 the region of SST anomalies included in the *4xWEST* forcing. We note that, when forced with the  
 192 WEST SST patterns, CAM6 produces a weaker westward extension relative to the *CTRL* experiment  
 193 (not shown). This suggests that tropical convection in CAM6 may be less effective in generating  
 194 subtropical high responses, likely due to differences in the diabatic heating profiles (R. Chen et  
 195 al., 2022). Therefore, the *4xWEST* forcing is chosen to enhance the simulated WPSH's westward  
 196 extension relative to the control simulation, which produces a WPSH westward extension of 134.9°E  
 197 and 128.7°E for COMP1 and COMP2, respectively. We illustrate this contribution by comparing  
 198 the difference in the 850-hPa geopotential heights between the spatially adjusted experiments and  
 199 the *CTRL* experiment. Figure 1 illustrates the forcing domains for the experiments listed in Table 1.

200 Table 1 lists and organizes all simulations analyzed in this study into four experimental sets.  
 201 Excluding the *CTRL* and *4xWEST* experiments, all other experiments comprise constraining SST  
 202 anomalies to select domains and zeroing SST forcing elsewhere. Experimental set 1 examines the in-  
 203 dividual contributions of the tropical Indian Ocean (TIO), Pacific Ocean (PAC), and Atlantic Ocean  
 204 (ATL) basin SST anomalies to the global COMP1 and COMP2 *4xWEST* forcings. These three  
 205 basins have previously been shown to play substantial roles in the development and maintenance  
 206 of the WPSH (Lu & Dong, 2001; B. Wu et al., 2010; W. Li et al., 2012; T. Li et al., 2017). In the  
 207 following sections, we will show that these basin contributions are not comparable between COMP1  
 208 and COMP2.

209 In experiment set 2, SSTs are constrained to the North Pacific basin (as defined in Table 1) and  
 210 examines whether Pacific SST magnitude, and consequently the strength of the zonal SST gradient  
 211 across the Pacific, drives the stark difference in response between the COMP1 *PAC* and COMP2  
 212 *PAC* forcings. For these experiments, the magnitude of negative *PAC* SST anomalies (-SSTA) for  
 213 COMP1 is doubled (*PACx2*) and then tripled (*PACx3*) to enhance the original COMP1 *PAC* zonal  
 214 SST gradient. Note that the *PACx2* and *PACx3* are conducted only for COMP1's *PAC* forcing.

215 Experiment sets 3 and 4 examine the individual contributions of intra-basin SST forcing by  
 216 constraining SSTs to the tropical (*TBAND*) and extratropical (*EXTBAND*) domains in the North  
 217 Pacific and Atlantic basins, respectively. The TBAND and EXTBAND domains were chosen based  
 218 on the distribution of COMP1 minus COMP2 SST differences (Figure 3c). Additionally, Jiang et al.  
 219 (2023) showed that the subtropical and extratropical regions may provide additional forcing along  
 220 with well-known forcing from the Pacific and Atlantic tropical belts. Therefore, we define *PAC*  
 221 *TBAND* and *PAC EXTBAND* intra-basin SST forcings for the North Pacific basin, and *ATL TBAND*  
 222 and *ATL EXTBAND* SST forcings for the Atlantic basin.

223 For all experiments, the change in WEI is taken relative to the mean control. Statistical sig-  
 224 nificance is determined via sample mean bootstrapping for a sample size of N=5 (see Figure S1).  
 225 Therefore, extensions westward of  $151.4^{\circ}\text{E}$  are considered statistically significant at the 95% level  
 226 for *4xWEST* simulations. Note also that no smoothing was applied to the edges of the SST patterns.  
 227 A comparison of the SST-forced simulations with smoothing versus no smoothing achieved similar  
 228 results (not shown). Finally, we acknowledge that the WPSH is maintained by coupled atmosphere-  
 229 ocean interactions (Seager et al., 2003). By using atmosphere-only simulations, our paper focuses  
 230 only on the atmosphere's response to the SST pattern.

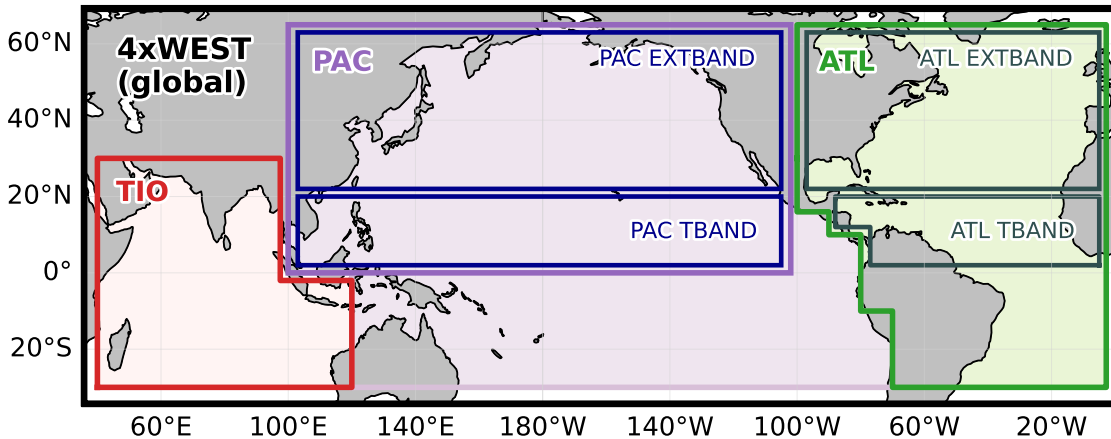


**Figure 1.** Outline of the main SST pattern forcing domains. The main domains include the tropical Indian Ocean (TIO, red), the North Pacific Ocean basin (PAC, purple), and the Atlantic Ocean basin (ATL, green).

**Table 1.** List of sea surface temperature forcing experiment sets, regional domains used, and brief descriptions of each experiment.

Experiment Set	Experiment Name	Description
1	1979-2019 Control (CTRL)	–
	4xWEST (Global)	–
	4xWEST minus ATL	ATL basin SSTs zeroed.
	4xWEST minus ATL,TIO	Both ATL and TIO basin SSTs zeroed.
2	North Pacific basin (PAC)	COMP1, COMP2 experiments.
	PACx2	COMP1 PAC -SSTA multiplied by 2, with lingering El Niño +SSTA changed to -SSTA.
	PACx3	As for PACx2, but -SSTA multiplied by 3.
3	PAC TBAND	0°-20°N, 100°E-160°W
	PAC EXTBAND	20°-60°N, 100°E-160°W
4	ATL only	North and South Atlantic basins
	ATL TBAND	0°-20°N, 100°W-0°
	ATL EXTBAND	20°-60°N, 100°W-0°

### 231 3 Two similar SST patterns belie two different SST forcing mechanisms

232 The COMP1 and COMP2 SST patterns have very similar SST patterns with only minor differences  
 233 in SST and Z850 anomalies. Figure 1 shows the SST and Z850 anomaly fields associated with  
 234 each season composite and the COMP1 minus COMP2 composite difference. As is characteristic of  
 235 summer seasons in which a strong westward extension of the Pacific subtropical high has occurred,  
 236 the underlying SST anomaly pattern consists of positive SST anomalies in the tropical Indian Ocean  
 237 and western North Pacific, negative SST anomalies in the central Pacific, a decaying El Niño or  
 238 developing La Niña within the equatorial eastern Pacific, and positive tropical North Atlantic SSTs.

239 Figure 2c indicate that most of the differences in SSTs between COMP1 and COMP2 lie in  
 240 the tropical and subtropical central and eastern Pacific, and the subtropical/extratropical Atlantic  
 241 regions. These differences are fairly small, ranging between -0.6°C to +0.6°C, and show no equiv-  
 242 alent effect in the Z850 anomaly composite difference (Figure 2f). The two SST composites also  
 243 show similarities in the monthly evolution of SSTs in key regions for WPSH development and  
 244 maintenance. Figure 3a and 3b show the YR(-1) and YR(0) monthly mean standardized anomalies  
 245 averaged over the TIO, extended ENSO domain (20°S-20°N, 160°E-120°W), WNP, and the TNA.  
 246 COMP1's D(-1)JF El Niño event is slightly stronger than that of COMP2, but both composites in-  
 247 dicate a comparable rate of decay of the winter El Niño. The June-August La Niña SST signal  
 248 averages -0.66°C for COMP1 and -0.78°C for COMP2. See Figure S2 for monthly SST evolution  
 249 for each year used to create the two SST composite patterns.

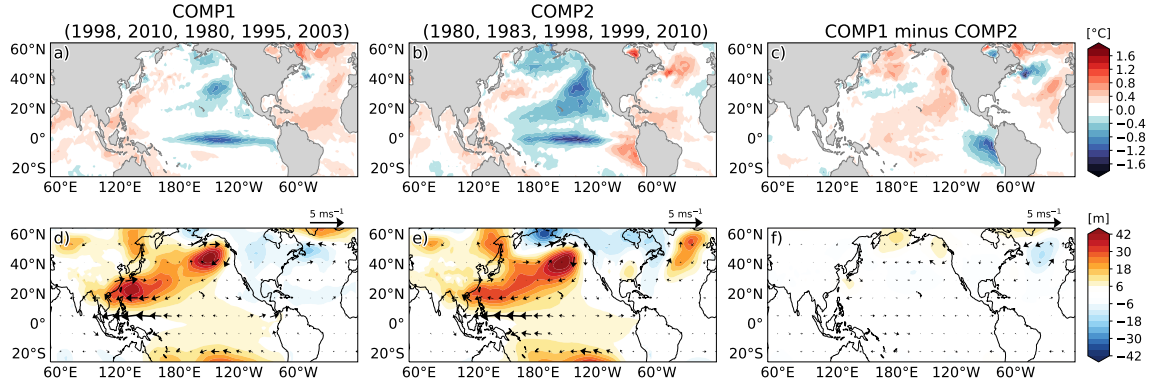


**Figure 2.** Composites and composite difference of June-August mean anomalous (a-c) SSTs, and (d-f) 850-hPa geopotential heights (shaded contours, m) with horizontal winds (quivers,  $\text{m s}^{-1}$ ) for COMP1 (1998, 2010, 1980, 1995, and 2003) and COMP2 (1980, 1983, 1998, 1999, and 2010).

Figures 3c and 3d illustrate the monthly evolution of standardized SST anomalies averaged over the tropical band between  $20^\circ\text{S}$ - $20^\circ\text{N}$ . The figures indicate that both COMP1 and COMP2 reflect an eastern Pacific (EP) La Niña-type signal, and even have a similar seasonal development of La Niña, following from a strong winter EP El Niño from the preceding year (Figure 2). The key difference between the two composites lies in the decay of the winter El Niño. In COMP1, the eastward migration of central Pacific negative SST anomalies doesn't occur until around April-May. In contrast, for COMP2, this eastward migration begins the year before (not shown) and can be observed in months January-March. In consequence of the earlier decay of COMP2's winter El Niño, negative SSTs  $>0.5^\circ\text{C}$  develop earlier in the summer, and are shown to spread further west into the central Pacific region.

In the CAM6 simulations, COMP1 and COMP2 show comparably strong westward extensions. Figures 4a and 4b illustrate the atmospheric response in 850-hPa geopotential heights to the *4xWEST* global SST forcing for COMP1 (Figure 4a) and COMP2 (Figure 4b). COMP1 and COMP2 produce WEI changes of  $-17^\circ$  and  $-23^\circ$ , respectively, statistically significant at the 95% confidence level from the *CTRL*. The two SST patterns also produce anomalous anticyclones of similar intensity over the WNP (not shown). This result is consistent with our observational analysis (Figures 2 and 3) and shows that COMP1 and COMP2 have similar impacts on the WPSH.

Despite similar responses to global SST anomalies, experiments constraining SST anomalies to individual basins give very different results, suggesting different sources of forcing. The first experimental set examines the relative contributions of three key regions for westward extensions simulated by the *4xWEST* experiments: the *ATL*, *TIO*, and *PAC*. In Figures 4c and 4d illustrate the COMP1 and COMP2 *4xWEST minus ATL* experiments, respectively, that illustrate the impact of removing *ATL* SSTs from the global SST forcing pattern. Figures 4e and 4f show the result

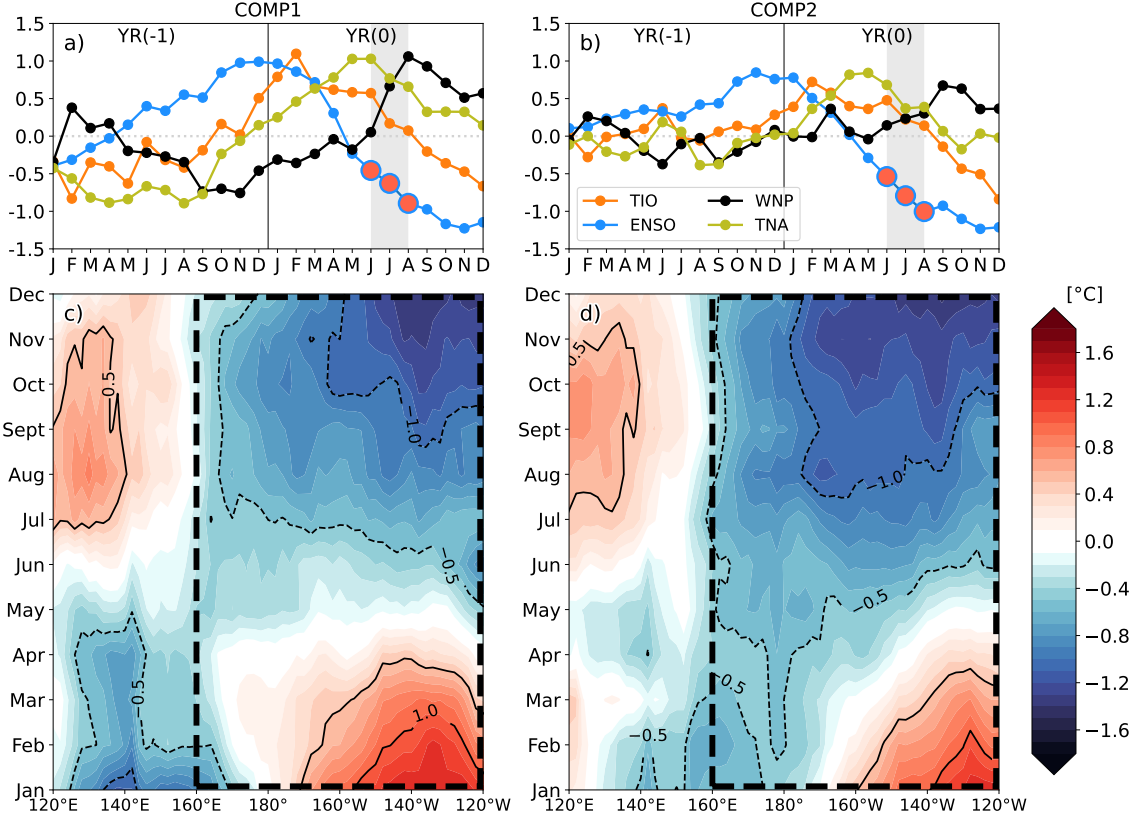


**Figure 3.** (a, b) Monthly mean standardized SSTs averaged over the TIO, WNP, equatorial eastern Pacific (ENSO), and the tropical North Atlantic (TNA) regions for the contemporaneous year (YR(0)) and the preceding year (YR(-1)). The YR(0) June-August (JJA) - which is the main focus of this study- is highlighted by the gray shading. ENSO values during JJA are highlighted by the large pink dots. (c, d) Longitude-time plot averaged over 20°S-20°N illustrates ENSO's monthly evolution during YR(0). Dashed box outlines the ENSO region, defined as 20°S-20°N and 160°E-120°W. The extended ENSO domain considers the longitudinal extent of the cold tongue anomalies (Williams & Patricola, 2018). The TNA region is defined as 0°-20°N, 100°W-0°.

of further removing *TIO* SSTs from the global SST forcing pattern, leaving just the *PAC* basins. Note that the westward extensions produced by COMP1 *4xWEST* falls off quickly once the ATL (and to a lesser extent, the *TIO*) is removed. In contrast, for the COMP2 *4xWEST* simulations, the *PAC* SSTs maintain the westward extension observed for its *4xWEST* simulation, with only a small change in WEI with the removal of *TIO*. This suggests that the COMP1 SST pattern forces westward extensions predominantly through inter-basin SST gradients while the COMP2 SST pattern forces westward extensions through intra-basin Pacific SST gradients.

The large-scale SST pattern's forcing of westward extensions can be viewed from the perspective of the zonal Pacific overturning atmospheric circulation. Figures 5a and 5b illustrate the meridional cross-section of the tropical atmospheric circulation averaged from 0°-30°N. Both COMP1

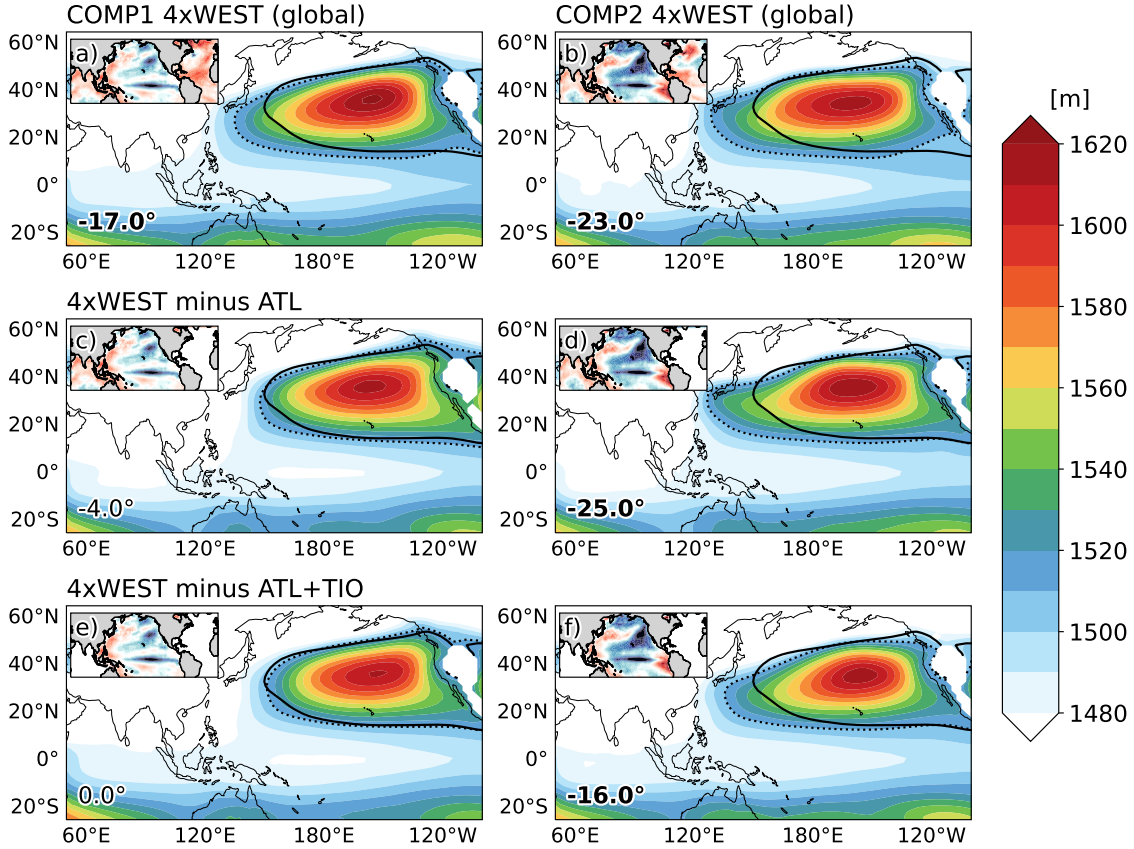


**Figure 4.** COMP1 versus COMP2 comparison of simulated 850-hPa geopotential heights in response to (a, b) *4xWEST*, (c, d) *4xWEST minus ATL*, (e, f) *4xWEST minus ATL+TIO* simulations. Inset plots showcase the respective SST forcing for each simulation. The solid black contour outlines the 1510-gph contour in *CTRL* simulation, while dashed contours outline the 1510-gph contour for the respective forcing simulations. The mean westward extent index (WEI) value produced by each experiment, expressed as the change relative to the *CTRL* WEI, is given in the bottom left corner of each subplot. Note that negative (positive) WEI changes indicate a westward extension (eastward retraction). WEI changes that are statistically significant at the 95% confidence level are highlighted in bold.

and COMP2 are characterized by strong subsidence over the central Pacific (the descending arm of the Walker Circulation) and ascent over the TIO and Atlantic regions. In the lower levels, the strong easterly flow associated with an enhanced WPSH and westward extension may be observed over the Indo-Pacific/WNP region between 100°E-180°. As the ATL and TIO forcings are removed, the descending arm supporting the strong lower-level easterlies over the central Pacific collapses for COMP1 (Figures 5c, 5e), but remains intact for COMP2 (Figures 5d, 5f). Note that when SSTs are further constrained, the WNP proves to be the smallest region that a statistically significant westward extension in COMP2. Therefore, for COMP1, the combined effect of the Atlantic SSTs and the tropical Pacific-Indian Ocean/WNP SST gradient lead to a robust westward extension of the STH.

So, why are the relative contributions of regional SSTs so different between the COMP1 and COMP2 SST patterns? From Figure 1c, we identify and examine three key regions of SST differences stand out in Figure 1c that may explain the difference in model response, which we further explore using the atmosphere-only CAM6 global climate model: the tropical and subtropical central and eastern Pacific SSTs, extratropical Pacific SSTs, and the subtropical and extratropical Atlantic SSTs.

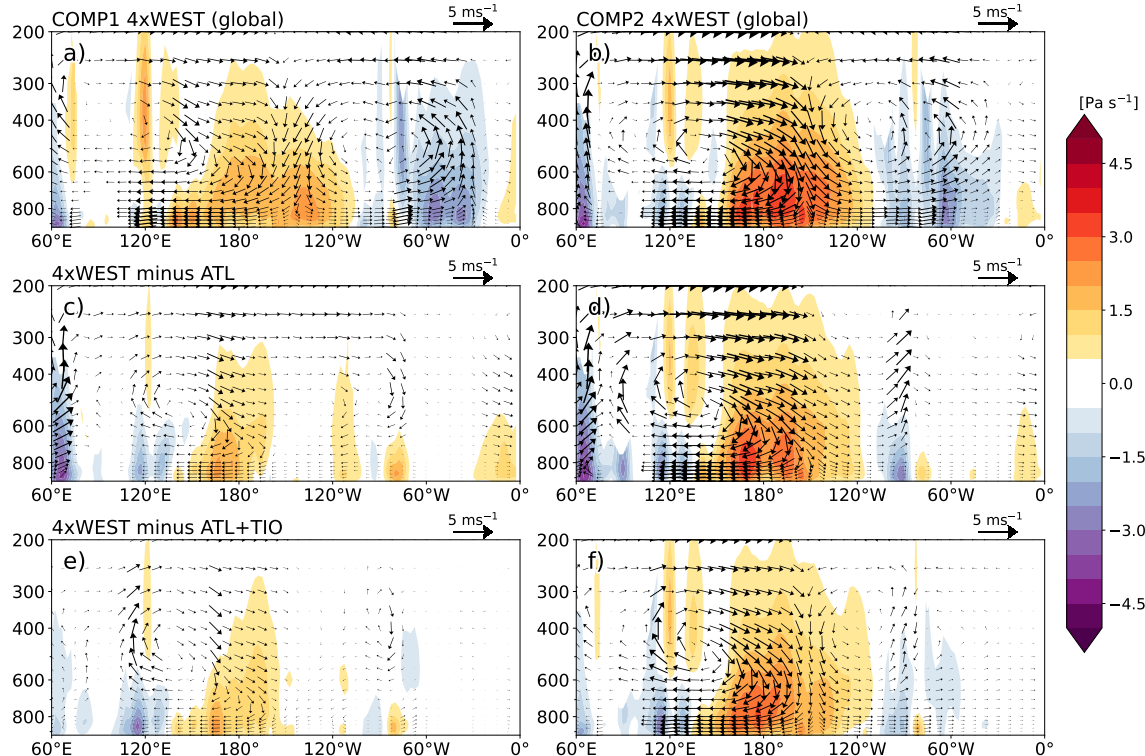


**Figure 5.** Meridionally-averaged longitude-pressure plots of vertical velocity anomalies (shading), with quivers representing the magnitude and direction of scaled vertical (x100) and zonal (x0.5) wind anomalies from the same experiments as Fig. 4. All plots are averaged over latitudes 0°–20°N.

298    **4 Tropical Pacific intra-basin SST forcing of westward extensions can be suppressed by**  
 299    **its extratropical SST forcing**

300    In the previous section, we showed that the relative contributions from remote SSTs (inter-  
 301    basin forcing) predominantly drive westward extensions in COMP1 simulations, while local Pacific  
 302    SSTs (intra-basin forcing) are the predominant driver in COMP2 simulations. Jiang et al. (2023)  
 303    observed that the *TIO* and *ATL* SSTs were strong drivers of westward extensions in seasons with  
 304    faster El Niño decays. The atmospheric response to the COMP1 SST pattern reflects the importance  
 305    of remote SSTs to its forcing mechanism and is consistent with Jiang et al. (2023)'s findings (Figures  
 306    5a, 5e, 5e). But COMP2 contradicts the profile for this mechanism, despite having a stronger zonal  
 307    SST gradient in the equatorial North Pacific than COMP1 (see Figure S3a) with arguably similar El  
 308    Niño decay rates (Figure 3). The results of this study and Jiang et al.'s results suggest that there is a  
 309    big difference in the forcing impact between COMP1 and COMP2 Pacific basin SSTs. In the second  
 310    experiment set, we test the differences between the COMP1 and COMP2 North Pacific SST forcing.

311    Figure 6 compares the simulated WPSH forced by North Pacific SST forcing (*PAC*) for COMP1  
 312    (Figure 6a,6e) and COMP2 (Figure 6d,6h). Negative SST anomalies in COMP1's *PAC* forcing were  
 313    doubled (*PACx2* in Figures 6b, 6f) and then tripled (*PACx3* in Figures 6c, 6g) to assess the impact  
 314    of cold central Pacific anomalies on COMP1's forcing. Increasing the magnitude of the CP and  
 315    EP negative anomalies results in only a slight improvement in westward extension (Figure 6a, 6b),  
 316    suggesting that the distribution of negative CP and EP SST anomalies is one key reason for the strong  
 317    westward extension forced by COMP2's *PAC* experiment, presumably by increasing the zonal SST  
 318    gradient across the Pacific basin. These results are consistent with previous studies that show the  
 319    state and transition of the summer La Niña can play a major role in forcing the atmospheric response  
 320    over the WNP (Jong et al., 2020; H. Li et al., 2020; Jiang et al., 2023).

321    Hence, the distribution and strength of the tropical CP and EP negative SST anomalies alone do  
 322    not explain the stronger westward extension and anomalous anticyclone produced for the COMP2  
 323    *PAC* forcing (Figures 6d and 6h). There remains no significant westward shift in the presence of a  
 324    substantial zonal SST gradient in the tropical Pacific (for an SST profile, see Figure S3b). Therefore,  
 325    in experimental set 3, we examine the contributions of SSTs in the Pacific tropical band (*TBAND*),  
 326    between 0°-20°N, and subtropical and extratropical domain (*EXTBAND*) to the JJA westward ex-  
 327    tensions.

328    The SST anomalies from the Pacific tropical band alone produces a comparable westward ex-  
 329    tension in COMP1 and COMP2 (*PAC TBAND*; Figures 7a vs. 7b). Similarly, the *PAC EXTBAND*  
 330    forcings for both COMP1 and COMP2 produce negative Z850 anomalies and an anomalous cyclone  
 331    over the WNP. However, the COMP1 *PAC EXTBAND* forces a stronger cyclonic flow, likely from  
 332    the broader spread of positive SST anomalies along the western boundary. Similar observations have

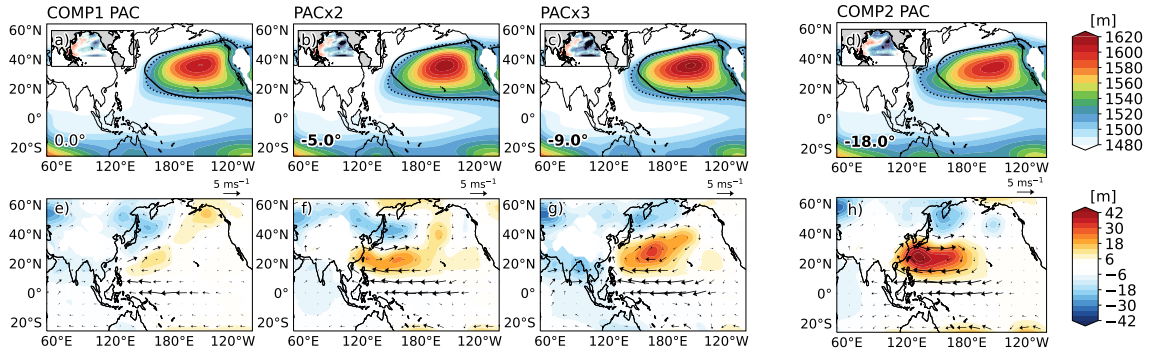


**Figure 6.** Simulation response in 850-hPa geopotential heights (top panels) and height anomalies relative to *CTRL* (bottom panels) to COMP1's (a, e) *PAC*, (b, f) *PACx2*, and (c, g) *PACx3*, compared to (d, h) COMP2's *PAC* experiment.

been made by Jiang et al. (2023). COMP1's *PAC EXTBAND* similarly produces an anomalous WNP cyclone, but the strength of this cyclone is curtailed by anomalous anticyclonic flow further north. Figure 7e shows the mean Z850 anomaly over the WNP for the *PAC TBAND* and *PAC EXTBAND*, and the net *TBAND+EXTBAND* forcing for both COMP1 and COMP2. For COMP1, the net *PAC* forcing reflects the suppression of the *PAC TBAND* forcing by *PAC EXTBAND* and produces similar Z850 anomalies as those forced by COMP1 *PAC* (Figure 5e). For COMP2, the relatively stronger forcing by COMP2 *TBAND* is enough to withstand forcing from its *EXTBAND*. Therefore, a key difference in the inter-basin versus intra-basin forcing of COMP1 and COMP2 stems from the difference in net Pacific forcing.

## 5 Remote Atlantic SST forcing drives westward extensions when the local net Pacific forcing is weak

From experimental sets 2 and 3, we have shown that the net contributions between the *PAC* and *ATL* basin SSTs may vary depending on the net *PAC* forcing. When *PAC TBAND* is much stronger than *PAC EXTBAND*, the westward extensions are driven predominantly by intra-basin *PAC* SST forcing. When the *PAC TBAND* is suppressed by *PAC EXTBAND*, the *ATL* and *TIO* SSTs (and hence inter-basin SSTs) predominantly force the westward extensions. Since the *TIO* forcing for COMP1 and COMP2 are identical (see Figure S4), the remaining SST difference lies with the *ATL*. So, are the *ATL* forcings significantly different between COMP1 and COMP2?

The results of the fourth experimental set show that the *ATL* SST forcing has comparable impacts on the WPSH's westward extension for both COMP1 and COMP2. Despite a clear difference between the COMP1 and COMP2 *ATL* SST patterns, both forcings produce a WEI change of  $-15^{\circ}\text{E}$  (Figures 8a, 8b). The key mechanism underlying the Atlantic forcing of WNP westward extensions

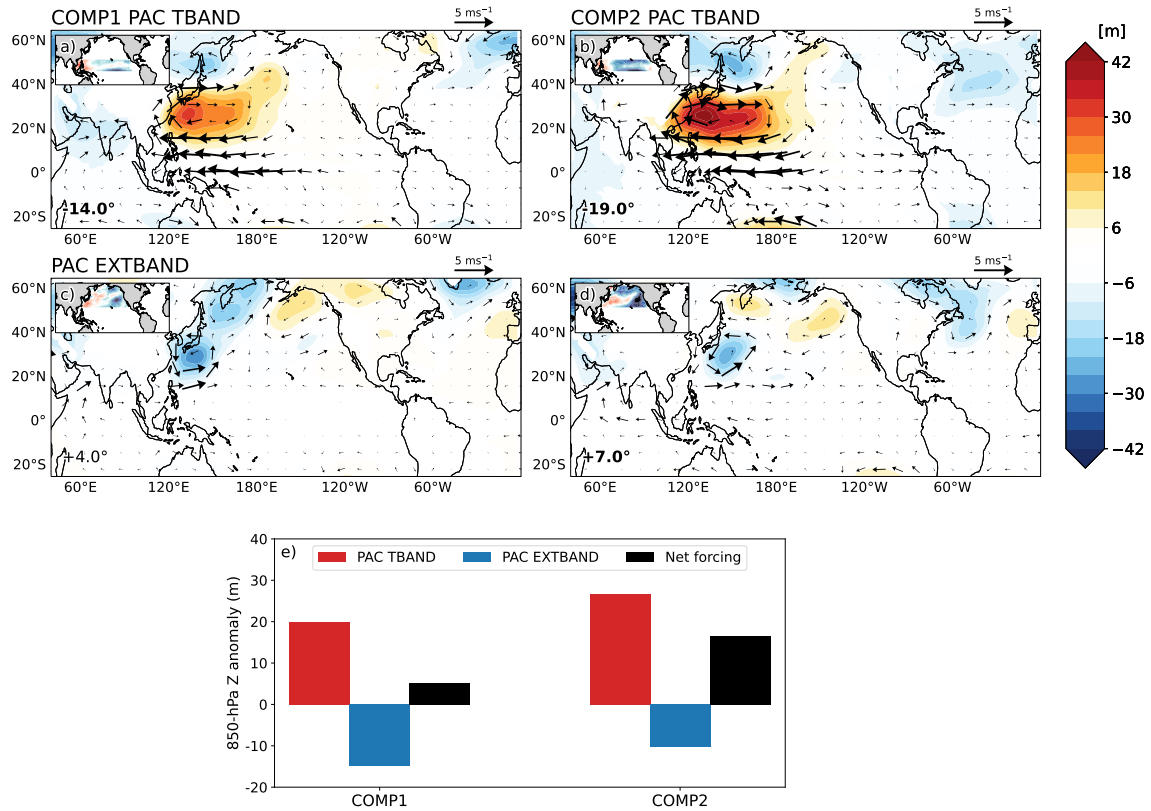


**Figure 7.** COMP1 versus COMP2 comparison of simulated 850-hPa geopotential height anomaly response to the forcing domains (a, b) *PAC TBAND*, and (c, d) *PAC EXTBAND*. e) Mean 850-hPa geopotential anomaly averaged over 10°-30°N and 100°E-180° for COMP1's and COMP2's Pacific *TBAND* and *EXTBAND* simulations.

355 comprises the forcing of an anomalous low-level cyclonic circulation, strong westerlies, and nega-  
 356 tive Z850 anomalies over the western North Atlantic. This atmospheric response likely spurs strong  
 357 ascent (see Figure 5a) which in turn forces strong subsidence over the WNP. When the *ATL* forcing  
 358 is divided into the *ATL TBAND* and *ATL EXTBAND* domains, the *ATL TBAND* proves to be the key  
 359 contributor to the larger *ATL* pattern (Figures 8c, 8d), consistent with studies that show that the trop-  
 360 ical Atlantic SSTs can substantially force the WNP anomalous cyclone and, consequently, westward  
 361 extensions (Lu & Dong, 2005; Hong et al., 2014; Zuo et al., 2019). The COMP2 *ATL TBAND* pro-  
 362 duces a slightly weaker extension compared to COMP1. Since the *ATL EXTBAND* forcings show  
 363 no significant westward extensions, the difference in the *ATL TBAND* forcings is attributed to the  
 364 widespread positive tropical North Atlantic SST anomalies in COMP1 that may drive a stronger  
 365 response over the western North Atlantic.

366 Unlike the net Pacific forcing of westward extensions, the net forcing from COMP2's Pacific (-  
 367 17°E) and Atlantic (-15°E) SSTs do not add linearly to recover its original 4xWEST forcing (-23°E)  
 368 (Figures 4b, 6d, 8b). The strong relative contributions from both the Pacific and Atlantic basins  
 369 clearly explain why COMP2 provides a stronger westward extension than COMP1. But, if the two  
 370 basins provide comparable impacts on the WPSH's westward extension, why does one basin show  
 371 a stronger forcing over the other? We suggest that, in contemporaneous forcing experiments, the  
 372 location of the forcing relative to the subsidence region matters. If local and remote SST forcings  
 373 are similar (as in the case of COMP2), the westward extensions are more likely to be driven by  
 374 SST anomalies in close proximity to the WPSH. Idealized experiments (not shown) show that the  
 375 westward extensions are sensitive to zonal shifts of the zonal SST gradient. Studies such as Jiang et  
 376 al. (2023) also imply this sensitivity, as cases in which the westward reach of equatorial Pacific cold  
 377 SST anomalies (and thus stronger zonal SST gradient) also produce a stronger forcing of WPSH  
 378 westward extensions.

## 379 6 Discussion and Conclusion

380 Many studies have highlighted the importance of SSTs in driving the WPSH's zonal variability.  
 381 Many have concluded that the tropical Indian and equatorial eastern Pacific SST variability are key  
 382 drivers of the WPSH's zonal extensions (B. Wang et al., 2013; H. Li et al., 2020). In this study,  
 383 we examined which SSTs across the Indian and Pacific Oceans matter for the westward extensions  
 384 by progressively constraining the SST forcing within atmosphere-only CESM2 model simulations.  
 385 The simulated WPSH's response to our forcing simulations is outlined in Table 2, and our key  
 386 conclusions are summarized as follows:

- 387 1. In comparing two very similar SST patterns (COMP1 and COMP2), we find that the large-  
 388 scale zonal inter-basin SST gradient that characterizes decaying El Niño and developing

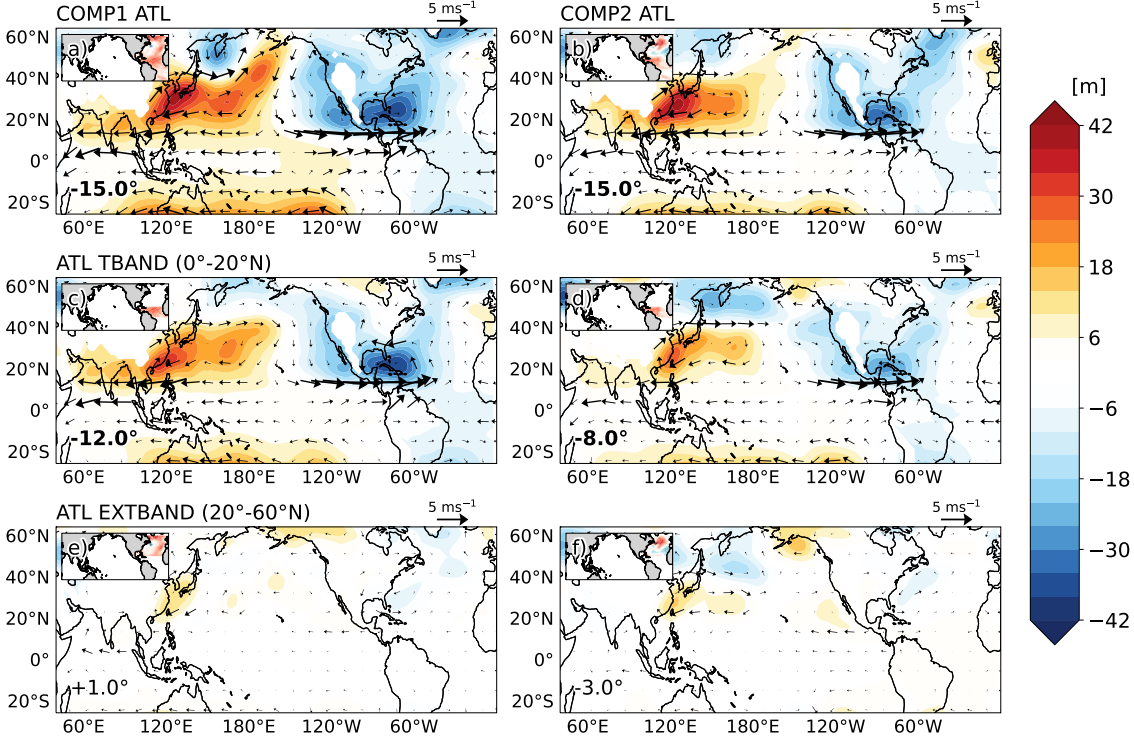


**Figure 8.** COMP1 versus COMP2 comparison of simulation response to experiments (a, b) ATL only, (c, d) ATL TBAND, and (e, f) ATL EXTBAND.

389 La Niña summers, is not always the predominant driver of the WPSH's westward exten-  
 390 sions. While COMP1 and COMP2 force comparable westward extensions, the relative con-  
 391 tributions from remote SSTs (inter-basin forcing) predominantly drive westward extensions  
 392 in COMP1 simulations, while local Pacific SSTs (intra-basin forcing) are the predominant  
 393 driver in COMP2 simulations.

- 394 2. One key reason for the difference in net contributions is likely due to differences in state  
 395 of the summer El Niño decay. The meridional spread and magnitude of central Pacific and  
 396 eastern Pacific negative SST anomalies, and even the presence of lingering El Niño-related  
 397 positive SST anomalies, weakens the Pacific zonal SST gradient in COMP1. However, this  
 398 only partially explains the inter-basin SST forcing of westward extensions by the COMP1  
 399 SST pattern. The second key reason is that the SSTs north of 20°N tends to force anomalous  
 400 cyclonic circulation over the WNP. In COMP1, the Pacific TBAND forcing of westward  
 401 extensions is completely suppressed by its PAC EXTBAND forcing, while COMP2's Pacific  
 402 TBAND forcing is strong enough to withstand suppression from it's PAC EXTBAND forcing.  
 403 3. When the net PAC forcing is weak, the Atlantic SST forcing drives the westward extensions.  
 404 The COMP1 and COMP2 SST patterns show that a warm ATL TBAND forces significant  
 405 westward extensions. Note that the PAC and ATL forcing simulations show comparable forc-

**Table 2.** Summary of the mean westward extension for each experiment, expressed as a change from the CTRL simulation. Negative (positive) values indicate a westward extension (eastward retraction). As with prior figures, values highlighted in bold represent statistical significance at the 95% confidence level.

Experiment	COMP1 WEI	COMP2 WEI
4xWEST (Global)	<b>-17°</b>	<b>-23°</b>
4xWEST minus ATL	-4°	<b>-25°</b>
4xWEST minus ATL,TIO	0°	<b>-16°</b>
PAC	0°	<b>-18°</b>
PACx2	<b>-5°</b>	—
PACx3	<b>-9°</b>	—
PAC TBAND	<b>-14°</b>	<b>-19°</b>
PAC EXTBAND	0°	-2°
ATL only	<b>-15°</b>	<b>-15°</b>
ATL TBAND	<b>-12°</b>	<b>-8°</b>
ATL EXTBAND	+1°	-3°

406 ing of westward extensions, but do not contribute in equal portions to the original *4xWEST*  
 407 forcing, particularly for COMP2 (see Figure S5). Instead, they may alternate the driving role  
 408 of the Walker Circulation, depending on the net Pacific SST forcing, as illustrated by Figure  
 409 4. This suggests that the relative contributions of the tropical Indian Ocean, Pacific, and At-  
 410 lantic basins may be non-linear in nature. This may not be entirely surprising considering that  
 411 the individual basins can have considerable influence on each other (Hoerling et al., 2001;  
 412 Chikamoto et al., 2020; Hu & Fedorov, 2020; Park et al., 2023).

413 The results of this paper also has implications for understanding WPSH westward extension  
 414 variability and the sources of SST forcing. Jiang et al. (2023) showed that the westward extensions  
 415 are sensitive to the rate of development of ENSO and thus the strength of the tropical zonal SST  
 416 gradient with negative impacts from subtropical Pacific SSTs. Our study further shows that these  
 417 characteristics may also determine whether the westward extensions are driven predominantly by  
 418 inter-basin Atlantic SST forcing versus intra-basin Pacific SST forcing. Additionally, Hong et al.  
 419 (2014) observed that the influence of tropical Atlantic warming on the WPSH has strengthened in  
 420 recent over recent decades. Seager et al. (2019) observed that precipitation trends favor increased  
 421 precipitation over the western Pacific with decreased precipitation over the central Pacific, indicat-  
 422 ing a strengthening of the zonal equatorial Pacific SST gradient. Further work will examine the  
 423 contributions of a warmer tropical Atlantic and strengthened equatorial Pacific SST gradient to fu-  
 424 ture variability and thus predictability of WPSH zonal extensions. Tropical Atlantic warming has  
 425 been shown to induce a La Niña-like pattern (McGregor et al., 2014; Chikamoto et al., 2020; Fosu et  
 426 al., 2020; Park et al., 2023). It could be possible in a fully-coupled framework, that remote tropical

427      Atlantic warming and the Atlantic's forced development of a La Niña may promote WPSH intensification.  
 428      In addition, the pattern of Atlantic warming in COMP1 is similar to the positive phase of  
 429      the Atlantic Multidecadal Variability (AMV) and provides further motivation for understanding of  
 430      the remote impacts of the Atlantic Ocean on WPSH development.

## 431      7 Open Research

432      The SST forcing files and model builds used in this analysis (Jones et al., 2023) are available  
 433      at the Zenodo repository <https://doi.org/10.5281/zenodo.10127842>. The ERA5 re-  
 434      analysis dataset (Hersbach et al., 2017) is publicly available through the Copernicus Climate Data  
 435      Store (<https://cds.climate.copernicus.eu>). The previous and current versions of the  
 436      CESM2 global climate model (UCAR, 2018) is freely available to the public and may be found at  
 437      <https://www.cesm.ucar.edu/models/cesm2/>.

## 438      Acknowledgments

439      This research was supported by the National Science Foundation (NSF) Faculty Early-Career De-  
 440     velopment Program (CAREER) Award 1945113. We would like to acknowledge high-performance  
 441      computing support from Cheyenne (doi:10.5065/D6RX99HX) provided by NCAR's Computational  
 442      and Information Systems Laboratory, sponsored by the NSF. Finally, we thank all the scientists,  
 443      software engineers, and administrators who contributed to the development of CESM2. We also  
 444      thank the Editor and Reviewers for the helpful comments and suggestions that helped to improve  
 445      the quality of our publication.

## 446      References

- 447      Camp, J., Scaife, A. A., & Heming, J. (2018). Predictability of the 2017 North Atlantic hurricane  
 448      season. *Atmospheric Science Letters*, 19(5), e813. <https://doi.org/10.1002/asl.813>.
- 449      Chaluvadi, R., Varikoden, H., Mujumdar, M., & Ingle, S. (2021). Variability of West Pacific subtrop-  
 450      ical high and its potential importance to the Indian summer monsoon rainfall. *International*  
 451      *Journal of Climatology*, 41(7), 4047–4060. <https://doi.org/10.1002/joc.7057>.
- 452      Chang, C., Zhang, Y., & Li, T. (2000). Interannual and interdecadal variations of the  
 453      East Asian summer monsoon and tropical Pacific SSTs. Part I: Roles of the sub-  
 454      tropical ridge. *Journal of Climate*, 13(24), 4310–4325. [https://doi.org/10.1175/1520-0442\(2000\)013%3C4310:IAIVOT%3E2.0.CO;2](https://doi.org/10.1175/1520-0442(2000)013%3C4310:IAIVOT%3E2.0.CO;2).
- 456      Chen, M., Yu, J.-Y., Wang, X., & Jiang, W. (2019). The changing impact mechanisms of a diverse El  
 457      Niño on the western Pacific subtropical high. *Geophysical Research Letters*, 46(2), 953–962.  
 458      <https://doi.org/10.1029/2018GL081131>.
- 459      Chen, R., Simpson, I. R., Deser, C., Wang, B., & Du, Y. (2022). Mechanisms behind the springtime

- 460                   north pacific ENSO teleconnection bias in climate models. *Journal of Climate*, 35(23), 4091–  
 461                   4110. <https://doi.org/10.1175/JCLI-D-22-0304.1>.
- 462                   Chen, Z., Wen, Z., Wu, R., & Du, Y. (2017). Roles of tropical SST anomalies in modulating the  
 463                   western north Pacific anomalous cyclone during strong La Nicaying years. *Climate Dynamics*,  
 464                   49, 633–647. <https://doi.org/10.1007/s00382-016-3364-4>.
- 465                   Chen, Z., Wen, Z., Wu, R., Lin, X., & Wang, J. (2016). Relative importance of tropical SST  
 466                   anomalies in maintaining the western North Pacific anomalous anticyclone during El Niño to  
 467                   La Niña transition years. *Climate Dynamics*, 46, 1027–1041. <https://doi.org/10.1007/s00382-015-2630-1>.
- 469                   Chikamoto, Y., Johnson, Z. F., Wang, S.-Y. S., McPhaden, M. J., & Mochizuki, T. (2020). El  
 470                   Niño?Southern Oscillation Evolution Modulated by Atlantic Forcing. *Journal of Geophysical  
 471                   Research: Oceans*, 125(8), e2020JC016318. <https://doi.org/10.1029/2020JC016318>.
- 472                   Danabasoglu, G., Lamarque, J.-F., Bacmeister, J., Bailey, D., DuVivier, A., Edwards, J., ... others  
 473                   (2020). The community earth system model version 2 (CESM2). *Journal of Advances in  
 474                   Modeling Earth Systems*, 12(2), e2019MS001916. <https://doi.org/10.1029/2019MS001916>.
- 475                   Dong, X., & He, C. (2020). Zonal displacement of the Western North Pacific subtropical  
 476                   high from early to late summer. *International Journal of Climatology*, 40(11), 5029–5041.  
 477                   <https://doi.org/10.1002/joc.6508>.
- 478                   Dong, X., Lin, R., & Fan, F. (2017). Comparison of the two modes of the Western Pacific sub-  
 479                   tropical high between early and late summer. *Atmospheric Science Letters*, 18(4), 153–160.  
 480                   <https://doi.org/10.1002/asl.737>.
- 481                   Feng, J., & Chen, W. (2021). Roles of the north Indian Ocean SST and tropical North At-  
 482                   lantic SST in the latitudinal extension of the anomalous western North Pacific anticy-  
 483                   clone during the El Niño decaying summer. *Journal of Climate*, 34(21), 8503–8517.  
 484                   <https://doi.org/10.1175/JCLI-D-20-0802.1>.
- 485                   Feng, J., Chen, W., & Wang, X. (2020). Reintensification of the anomalous western North  
 486                   Pacific anticyclone during the El Niño Modoki decaying summer: Relative importance  
 487                   of tropical Atlantic and Pacific SST anomalies. *Journal of Climate*, 33(8), 3271–3288.  
 488                   <https://doi.org/10.1175/JCLI-D-19-0154.1>.
- 489                   Fosu, B., He, J., & Liguori, G. (2020). Equatorial Pacific warming attenuated by SST warming  
 490                   patterns in the tropical Atlantic and Indian Oceans. *Geophysical Research Letters*, 47(18),  
 491                   e2020GL088231. <https://doi.org/10.1029/2020GL088231>.
- 492                   Guan, W., Hu, H., Ren, X., & Yang, X.-Q. (2019). Subseasonal zonal variability of the western  
 493                   Pacific subtropical high in summer: climate impacts and underlying mechanisms. *Climate  
 494                   Dynamics*, 53(5), 3325–3344. <https://doi.org/10.1007/s00382-019-04705-4>.
- 495                   He, C., & Zhou, T. (2015). Responses of the western North Pacific subtropical high to global warm-  
 496                   ing under RCP4. 5 and RCP8. 5 scenarios projected by 33 CMIP5 models: The dominance

- 497 of tropical Indian Ocean–tropical western Pacific SST gradient. *Journal of Climate*, 28(1),  
 498 365–380. <https://doi.org/10.1175/JCLI-D-13-00494.1>.
- 499 Hersbach, H., Bell, B., Berrisford, P., Biavati, G., Horányi, A., Muñoz Sabater, J., ... others  
 500 (2017). Complete ERA5 from 1940: Fifth generation of ECMWF atmospheric reanalyses  
 501 of the global climate [Dataset]. Copernicus Climate Change Service (C3S) Data Store (CDS).  
 502 <https://doi.org/10.24381/cds.143582cf>.
- 503 Hersbach, H., Bell, B., Berrisford, P., Hirahara, S., Horányi, A., Muñoz Sabater, J., ... Thépaut,  
 504 J.-N. (2020). The ERA5 global reanalysis. *Quart. J. Roy. Meteor. Soc.*, 146(730), 1999–2049.  
 505 <https://doi.org/10.1002/qj.3803>.
- 506 Hoerling, M. P., Hurrell, J. W., & Xu, T. (2001). Tropical Origins for  
 507 Recent North Atlantic Climate Change. *Science*, 292(5514), 90–92.  
 508 <https://www.science.org/doi/abs/10.1126/science.1058582>.
- 509 Hong, C.-C., Chang, T.-C., & Hsu, H.-H. (2014). Enhanced relationship between the  
 510 tropical Atlantic SST and the summertime western North Pacific subtropical high after  
 511 the early 1980s. *Journal of Geophysical Research: Atmospheres*, 119(7), 3715–3722.  
 512 <https://doi.org/10.1002/2013JD021394>.
- 513 Hong, C.-C., Lee, M.-Y., Hsu, H.-H., Lin, N.-H., & Tsuang, B.-J. (2015). Tropical SST forcing on  
 514 the anomalous WNP subtropical high during July–August 2010 and the record-high SST in  
 515 the tropical Atlantic. *Climate Dynamics*, 45, 633–650. <https://doi.org/10.1007/s00382-014-2275-5>.
- 517 Hu, S., & Fedorov, A. V. (2020). Indian Ocean warming as a driver of the North Atlantic warming  
 518 hole. *Nature communications*, 11(1), 4785. <https://doi.org/10.1038/s41467-020-18522-5>.
- 519 Jiang, L., Chen, H.-C., Li, T., & Chen, L. (2023). Diverse Response of Western North Pacific  
 520 Anticyclone to Fast-Decay El Niño During Decaying Summer. *Geophysical Research Letters*,  
 521 50(7), e2022GL102612. <https://doi.org/10.1029/2022GL102612>.
- 522 Johnson, Z. F., Chavas, D. R., & Ramsay, H. A. (2022). Statistical framework for western North  
 523 Pacific tropical cyclone landfall risk through modulation of the western Pacific subtropical  
 524 high and ENSO. *Journal of Climate*, 1–32. <https://doi.org/10.1175/JCLI-D-21-0824.1>.
- 525 Jones, J. J., Chavas, D. R., & Johnson, Z. F. (2023, November). SST forcing files  
 526 and Model Builds for "Inter- basin versus intra-basin sea surface temperature forcing  
 527 of the Western North Pacific subtropical high's westward extensions" [Dataset]. Zenodo.  
 528 <https://doi.org/10.5281/zenodo.10127842>.
- 529 Jong, B.-T., Ting, M., Seager, R., & Anderson, W. B. (2020). ENSO teleconnections and impacts  
 530 on US summertime temperature during a multiyear La Niña life cycle. *Journal of Climate*,  
 531 33(14), 6009–6024. <https://doi.org/10.1175/JCLI-D-19-0701.1>.
- 532 Kosaka, Y., Xie, S.-P., Lau, N.-C., & Vecchi, G. A. (2013). Origin of seasonal predictability  
 533 for summer climate over the Northwestern Pacific. *Proceedings of the National Academy of*

- Sciences, 110(19), 7574–7579. <https://doi.org/10.1073/pnas.1215582110>.

Li, H., Xu, F., & Lin, Y. (2020). The impact of SST on the zonal variability of the western Pacific subtropical high in boreal summer. *Journal of Geophysical Research: Atmospheres*, 125(11), e2019JD031720. <https://doi.org/10.1029/2019JD031720>.

Li, T., Wang, B., Wu, B., Zhou, T., Chang, C.-P., & Zhang, R. (2017). Theories on formation of an anomalous anticyclone in western North Pacific during El Niño: A review. *Journal of Meteorological Research*, 31(6), 987–1006. <https://doi.org/10.1007/s13351-017-7147-6>.

Li, W., Li, L., Ting, M., & Liu, Y. (2012). Intensification of Northern Hemisphere subtropical highs in a warming climate. *Nature Geoscience*, 5(11), 830–834. <https://doi.org/10.1038/ngeo1590>.

Liu, Y., Wu, G., & Ren, R. (2004). Relationship between the subtropical anticyclone and diabatic heating. *Journal of Climate*, 17(4), 682–698. [https://doi.org/10.1175/1520-0442\(2004\)017%3C0682:RBTSAE%3E2.0.CO;2](https://doi.org/10.1175/1520-0442(2004)017%3C0682:RBTSAE%3E2.0.CO;2).

Lu, R. (2001). Interannual variability of the summertime North Pacific subtropical high and its relation to atmospheric convection over the warm pool. *Journal of the Meteorological Society of Japan. Ser. II*, 79(3), 771–783. <https://doi.org/10.2151/jmsj.79.771>.

Lu, R., & Dong, B. (2001). Westward extension of North Pacific subtropical high in summer. *Journal of the Meteorological Society of Japan. Ser. II*, 79(6), 1229–1241. <https://doi.org/10.2151/jmsj.79.1229>.

Lu, R., & Dong, B. (2005). Impact of Atlantic sea surface temperature anomalies on the summer climate in the western North Pacific during 1997–1998. *Journal of Geophysical Research: Atmospheres*, 110(D16). <https://doi.org/10.1029/2004JD005676>.

McGregor, S., Timmermann, A., Stuecker, M. F., England, M. H., Merrifield, M., Jin, F.-F., & Chikamoto, Y. (2014). Recent Walker circulation strengthening and Pacific cooling amplified by Atlantic warming. *Nature Climate Change*, 4(10), 888–892. <https://doi.org/10.1038/nclimate2330>.

Park, J.-H., Yeh, S.-W., Kug, J.-S., Yang, Y.-M., Jo, H.-S., Kim, H.-J., & An, S.-I. (2023). Two regimes of inter-basin interactions between the Atlantic and Pacific Oceans on interannual timescales. *npj Climate and Atmospheric Science*, 6(1), 13. <https://doi.org/10.1038/s41612-023-00332-3>.

Qian, W., & Shi, J. (2017). Tripole precipitation pattern and SST variations linked with extreme zonal activities of the western Pacific subtropical high. *International Journal of Climatology*, 37(6), 3018–3035. <https://doi.org/10.1002/joc.4897>.

Rodwell, M. J., & Hoskins, B. J. (2001). Subtropical anticyclones and summer monsoons. *Journal of Climate*, 14(15), 3192–3211. [https://doi.org/10.1175/1520-0442\(2001\)014%3C3192:SAASM%3E2.0.CO;2](https://doi.org/10.1175/1520-0442(2001)014%3C3192:SAASM%3E2.0.CO;2).

Seager, R., Cane, M., Henderson, N., Lee, D.-E., Abernathay, R., & Zhang, H. (2019). Strengthening tropical Pacific zonal sea surface temperature gradient consistent with rising greenhouse gases.

- 571                   *Nature Climate Change*, 9(7), 517–522. <https://doi.org/10.1038/s41558-019-0505-x>.
- 572 Seager, R., Murtugudde, R., Naik, N., Clement, A., Gordon, N., & Miller, J. (2003). Air-Sea Inter-  
573 action and the Seasonal Cycle of the Subtropical Anticyclones. *Journal of Climate*, 16(12),  
574 1948 - 1966. [https://doi.org/10.1175/1520-0442\(2003\)016;1948:AIATSC\\_2.0.CO;2](https://doi.org/10.1175/1520-0442(2003)016;1948:AIATSC_2.0.CO;2).
- 575 UCAR. (2018). Community Earth System Model (Version 2.0) [Software]. University Corporation  
576 for Atmospheric Research. <https://www.cesm.ucar.edu/models/cesm2/>.
- 577 Wang, B., Xiang, B., & Lee, J.-Y. (2013). Subtropical high predictability establishes a promising  
578 way for monsoon and tropical storm predictions. *Proceedings of the National Academy of  
579 Sciences*, 110(8), 2718–2722. <https://doi.org/10.1073/pnas.1214626110>.
- 580 Wang, X., Li, T., & He, C. (2021). Impact of the Mean State on El Niño–Induced Western North  
581 Pacific Anomalous Anticyclones during El Niño Decaying Summer in AMIP Models. *Journal  
582 of Climate*, 34(22), 9201–9217. <https://doi.org/10.1175/JCLI-D-20-0747.1>.
- 583 Williams, I. N., & Patricola, C. M. (2018). Diversity of ENSO Events Unified by Convective  
584 Threshold Sea Surface Temperature: A Nonlinear ENSO Index. *Geophysical Research Letters*,  
585 45(17), 9236-9244. <https://doi.org/10.1029/2018GL079203>.
- 586 Wu, B., Li, T., & Zhou, T. (2010). Relative Contributions of the Indian Ocean and Lo-  
587 cal SST Anomalies to the Maintenance of the Western North Pacific Anomalous Anticy-  
588 clone during the El Niño Decaying Summer. *Journal of Climate*, 23(11), 2974 - 2986.  
589 <https://doi.org/10.1175/2010JCLI3300.1>.
- 590 Wu, Q., Wang, X., & Tao, L. (2020). Interannual and interdecadal impact of Western North Pa-  
591 cific Subtropical High on tropical cyclone activity. *Climate Dynamics*, 54(3), 2237–2248.  
592 <https://doi.org/10.1007/s00382-019-05110-7>.
- 593 Xie, S.-P., Hu, K., Hafner, J., Tokinaga, H., Du, Y., Huang, G., & Sampe, T. (2009). Indian  
594 Ocean capacitor effect on Indo–western Pacific climate during the summer following El Niño.  
595 *Journal of climate*, 22(3), 730–747. <https://doi.org/10.1175/2008JCLI2544.1>.
- 596 Xie, S.-P., Kosaka, Y., Du, Y., Hu, K., Chowdary, J. S., & Huang, G. (2016). Indo-western Pacific  
597 Ocean capacitor and coherent climate anomalies in post-ENSO summer: A review. *Advances  
598 in Atmospheric Sciences*, 33(4), 411–432. <https://doi.org/10.1007/s00376-015-5192-6>.
- 599 Yuan, Y., & Yan, H. (2013). Different types of La Niña events and different responses of the  
600 tropical atmosphere. *Chinese Science Bulletin*, 58, 406–415. [https://doi.org/10.1007/s11434-012-5423-5](https://doi.org/10.1007/s11434-<br/>601 012-5423-5).
- 602 Zhou, T., Yu, R., Zhang, J., Drange, H., Cassou, C., Deser, C., ... others (2009). Why the western  
603 Pacific subtropical high has extended westward since the late 1970s. *Journal of Climate*,  
604 22(8), 2199–2215. <https://doi.org/10.1175/2008JCLI2527.1>.
- 605 Zuo, J., Li, W., Sun, C., & Ren, H.-C. (2019). Remote forcing of the northern tropical Atlantic  
606 SST anomalies on the western North Pacific anomalous anticyclone. *Climate Dynamics*, 52,  
607 2837–2853. <https://doi.org/10.1007/s00382-018-4298-9>.

**Figure 1.**

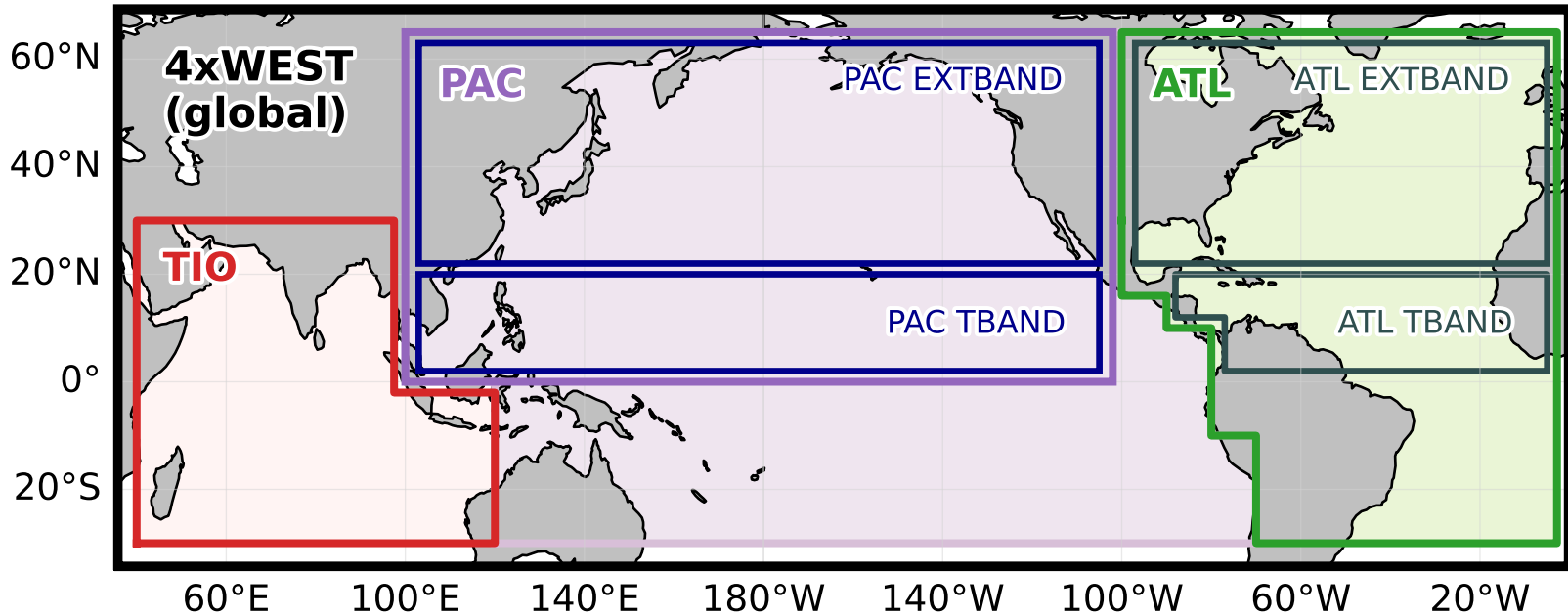
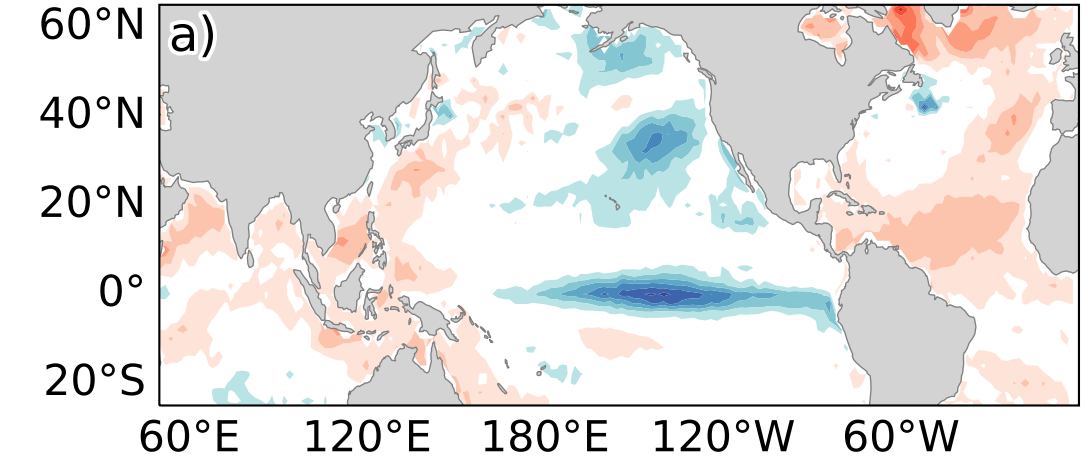


**Figure 2.**

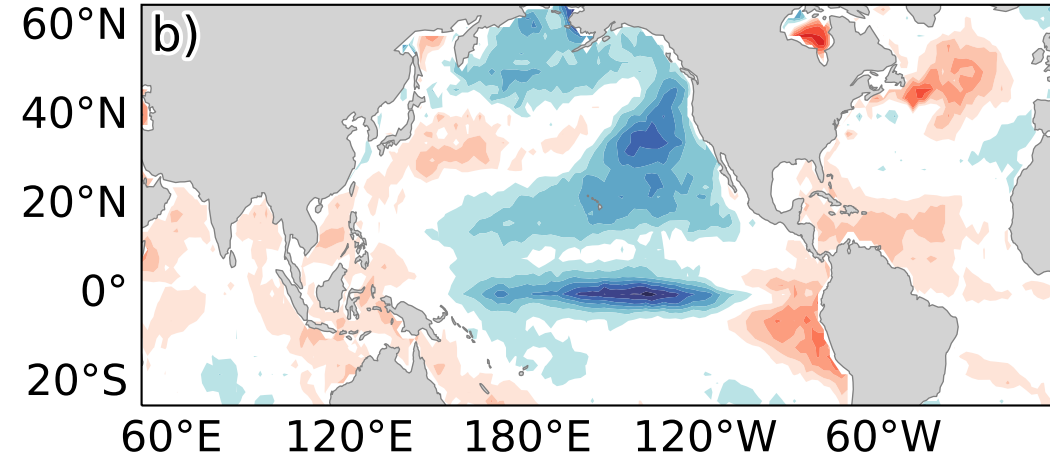
COMP1

(1998, 2010, 1980, 1995, 2003)

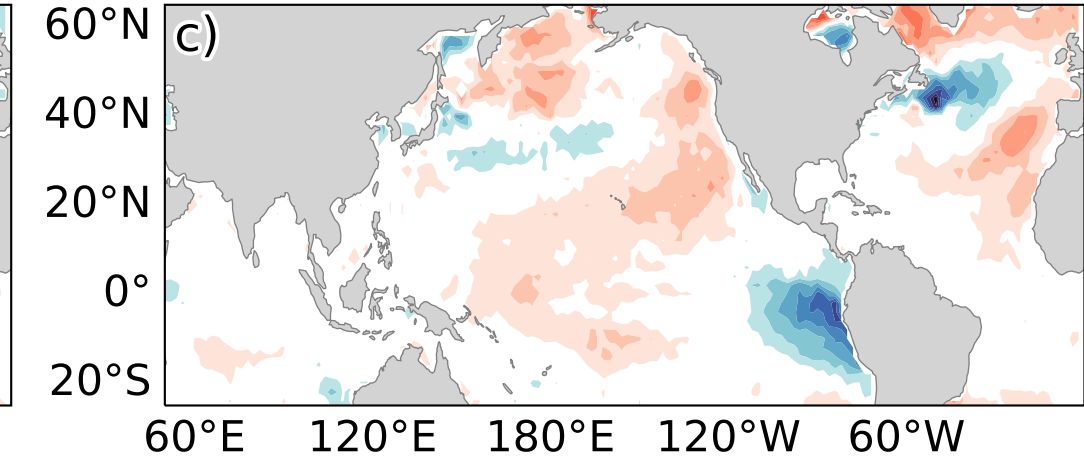


COMP2

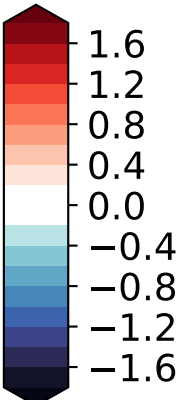
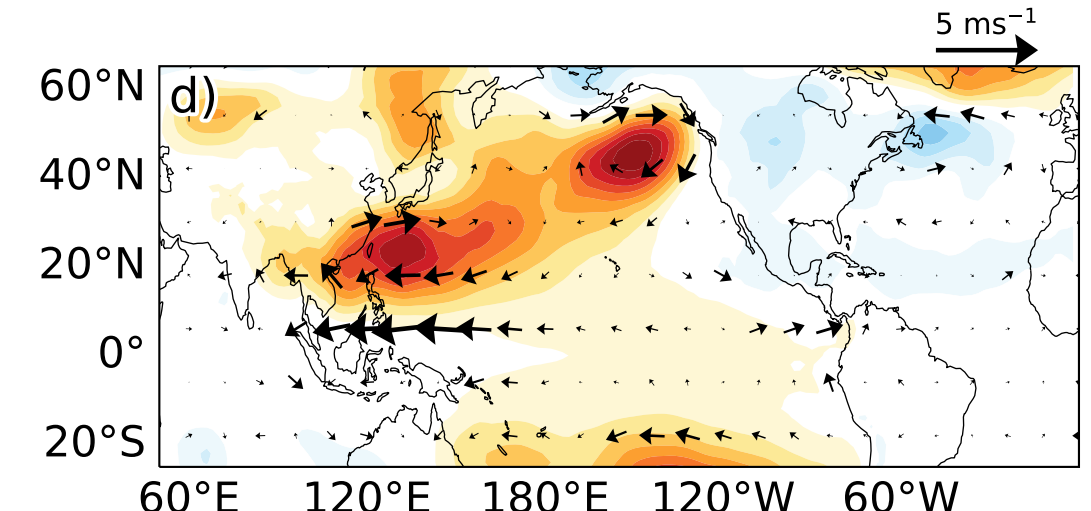
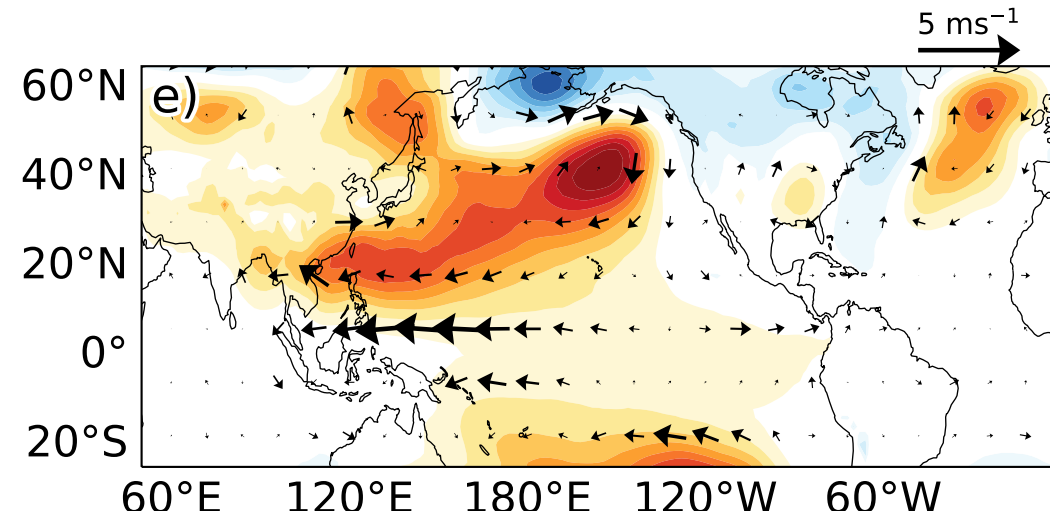
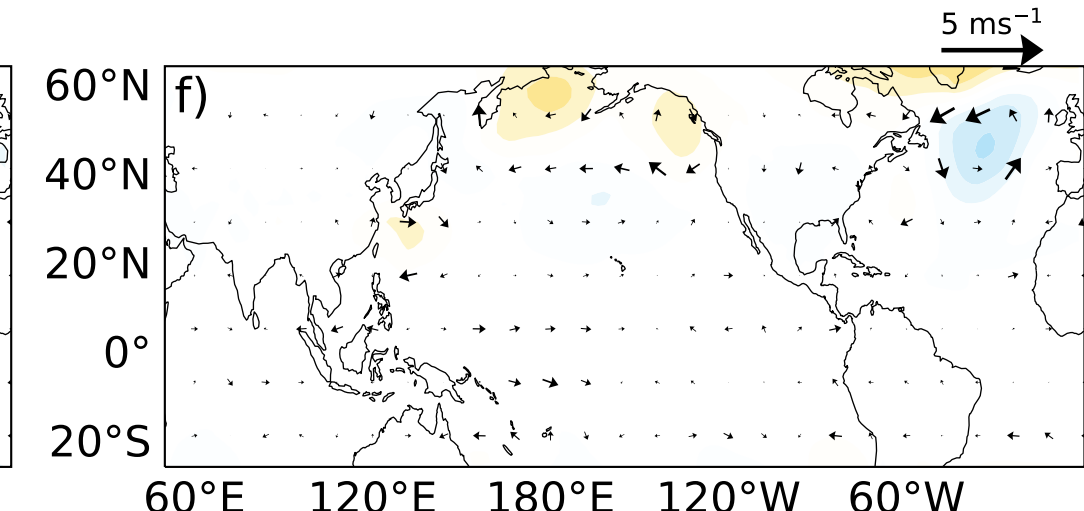
(1980, 1983, 1998, 1999, 2010)



COMP1 minus COMP2



[°C]

 $5 \text{ ms}^{-1}$  $5 \text{ ms}^{-1}$  $5 \text{ ms}^{-1}$ 

[m]

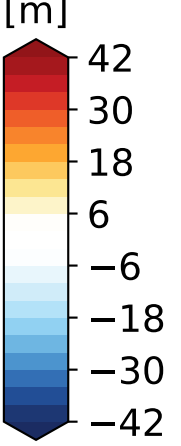
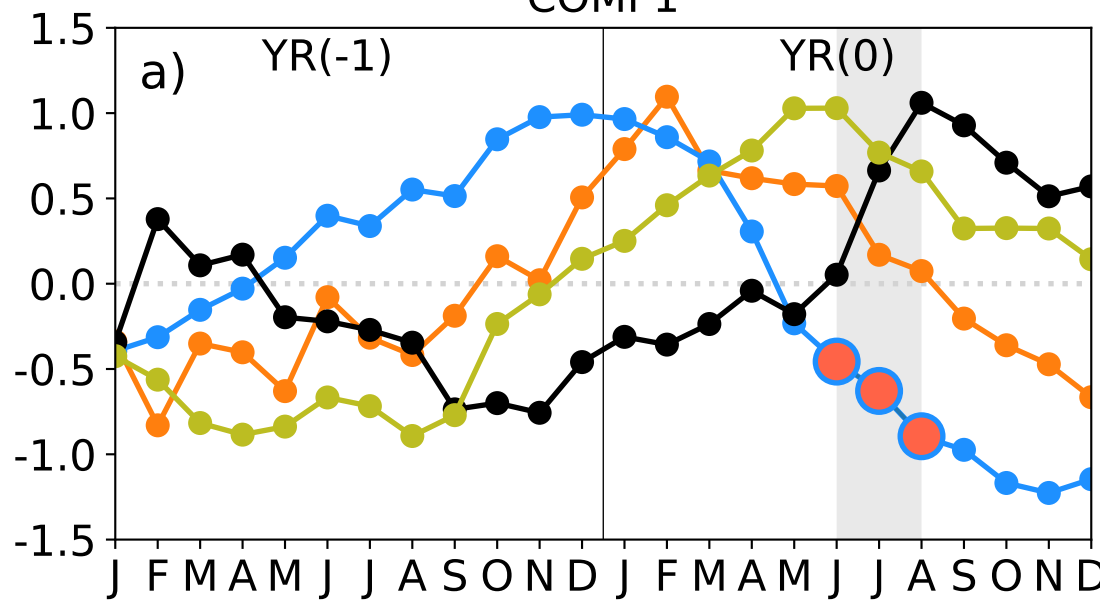
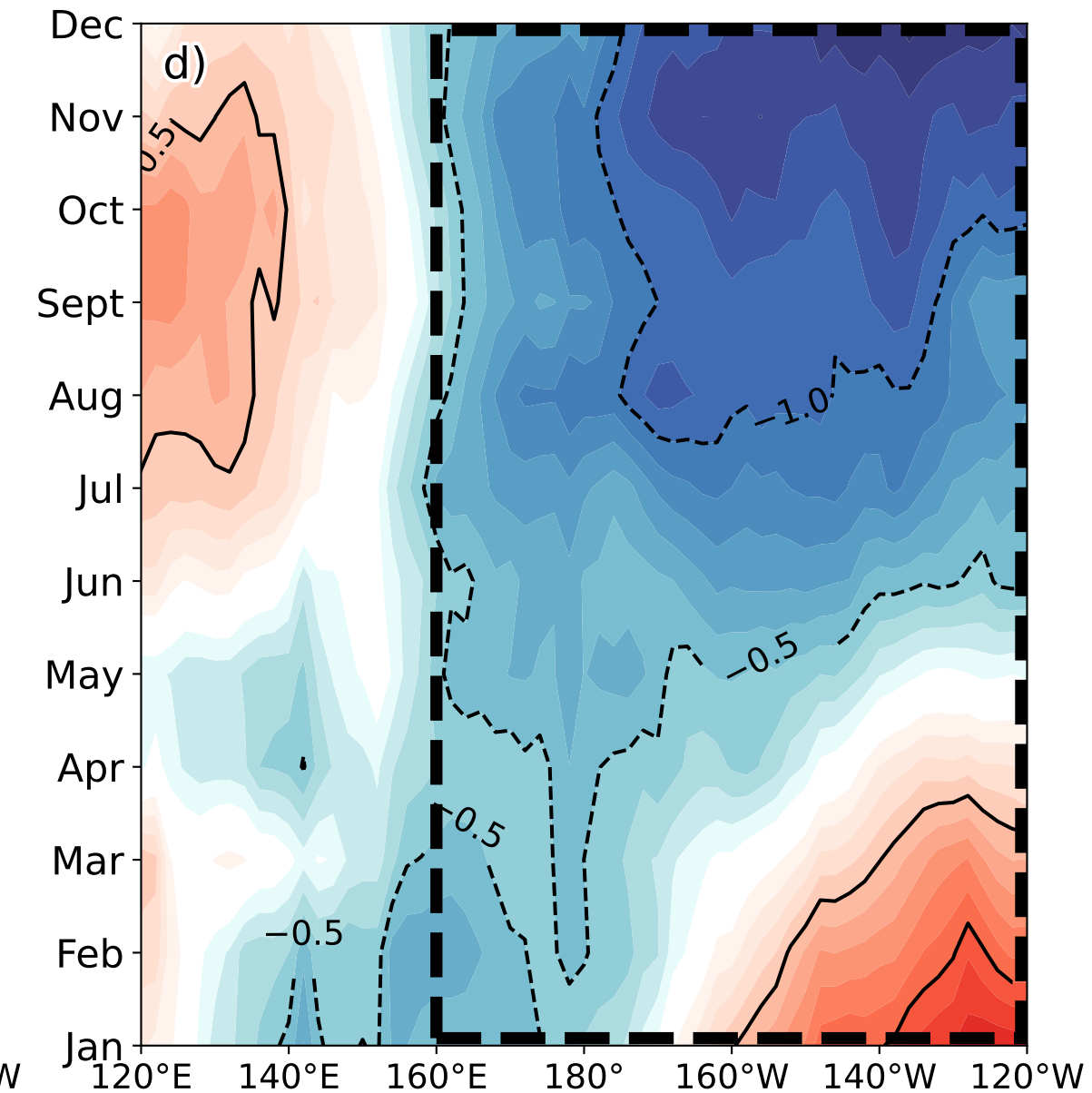
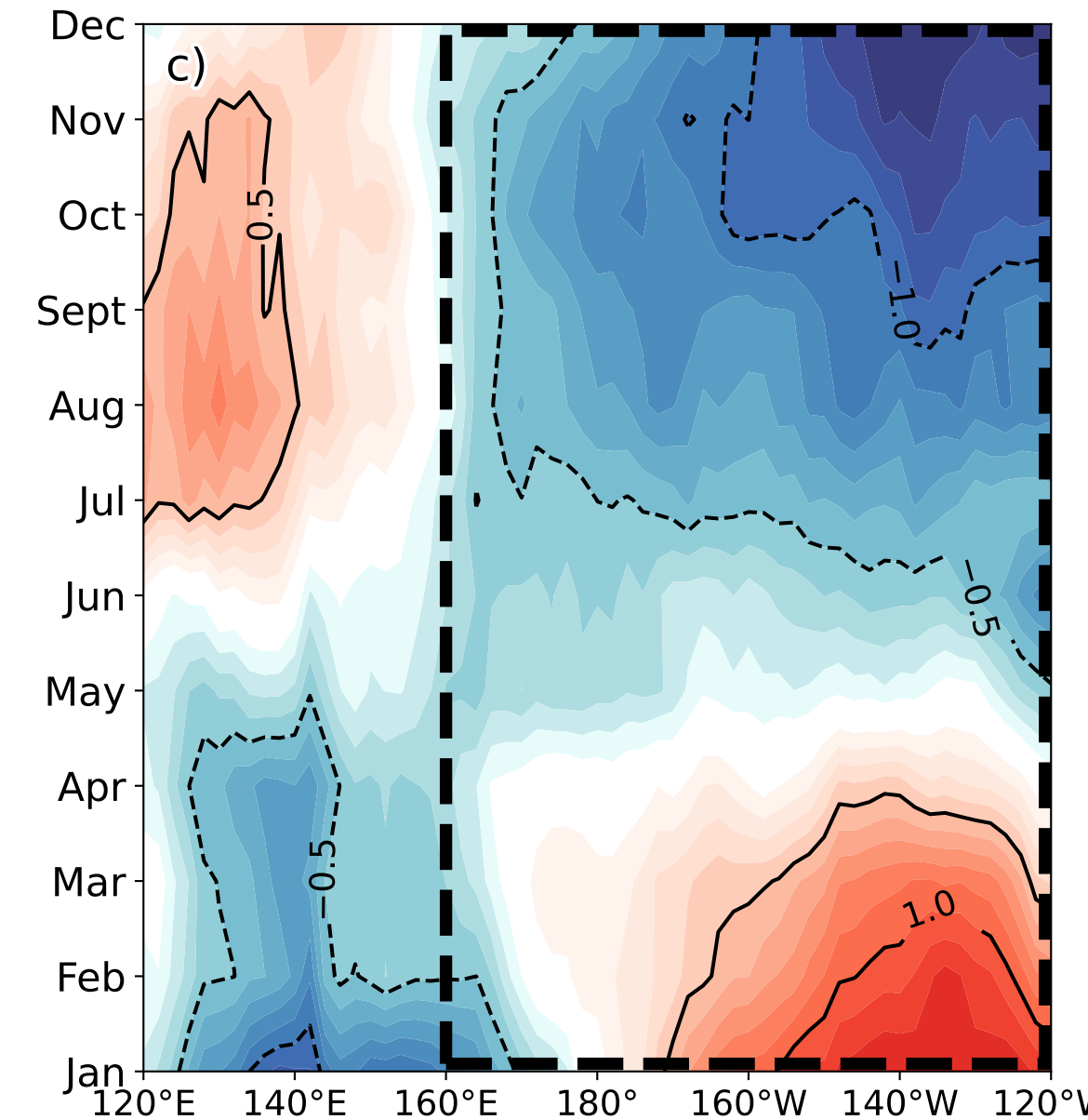
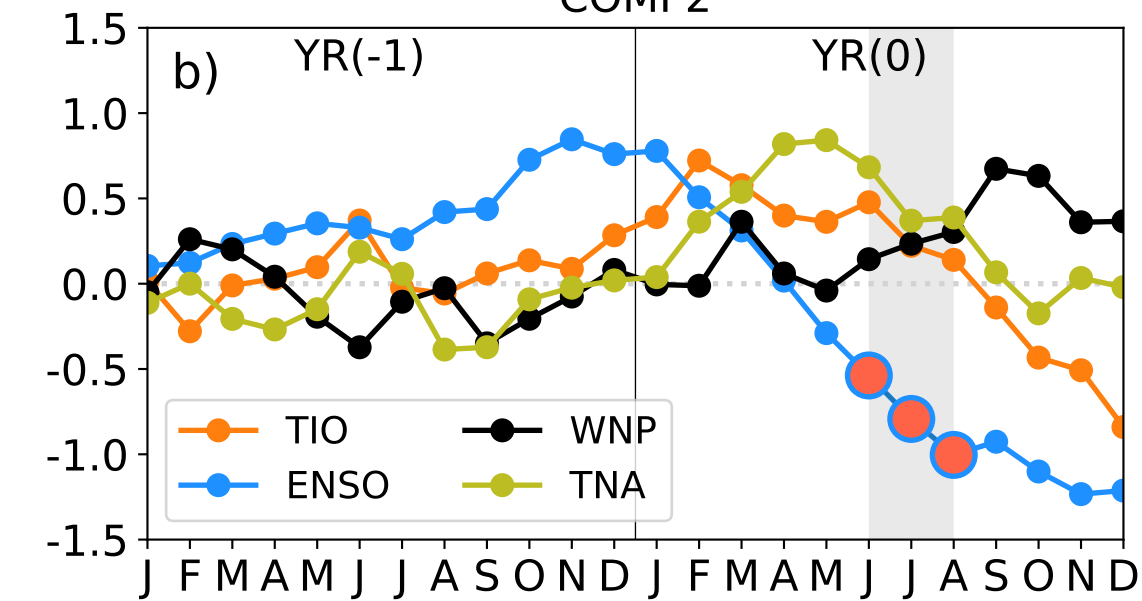


**Figure 3.**

COMP1



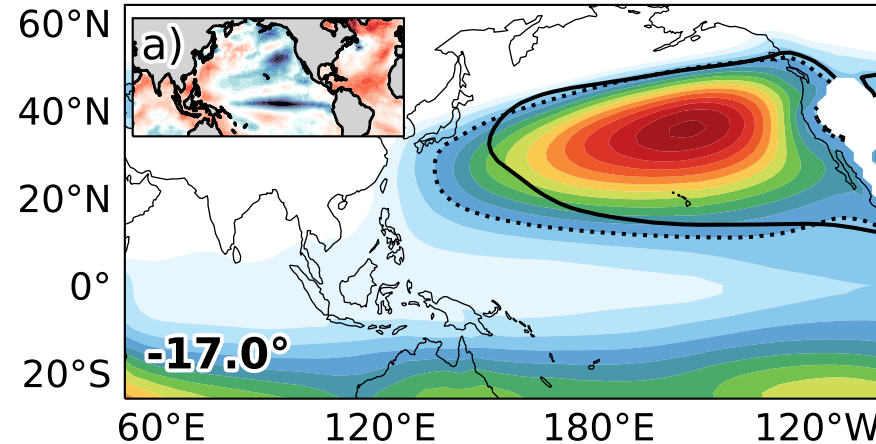
COMP2



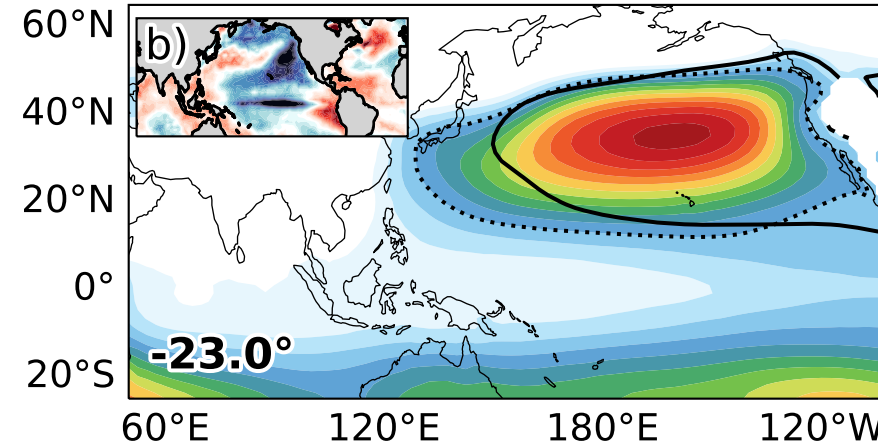
[°C]

**Figure 4.**

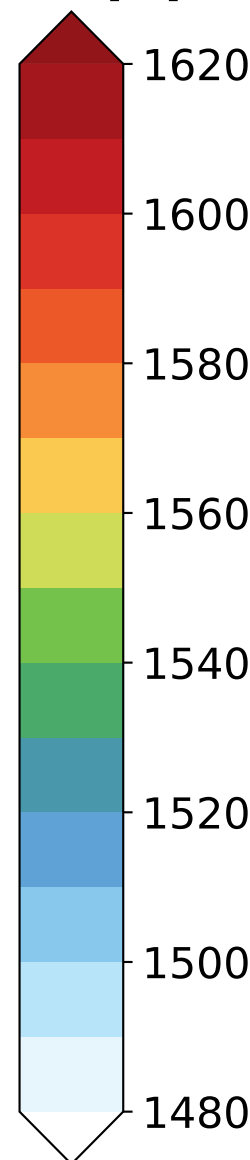
COMP1 4xWEST (global)



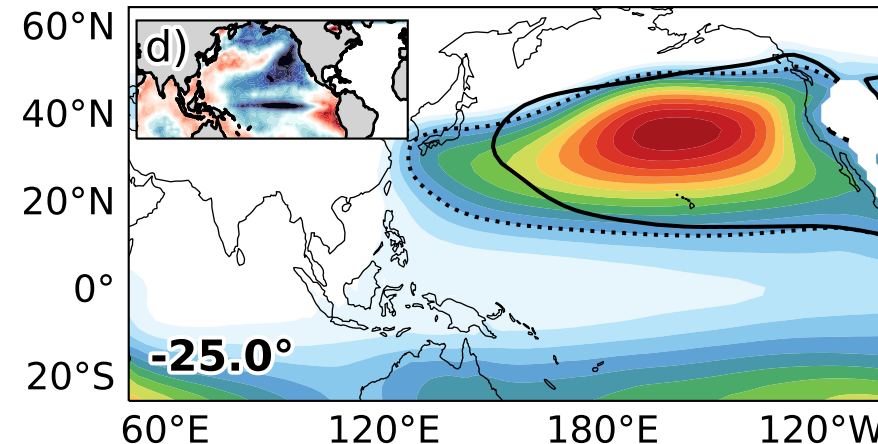
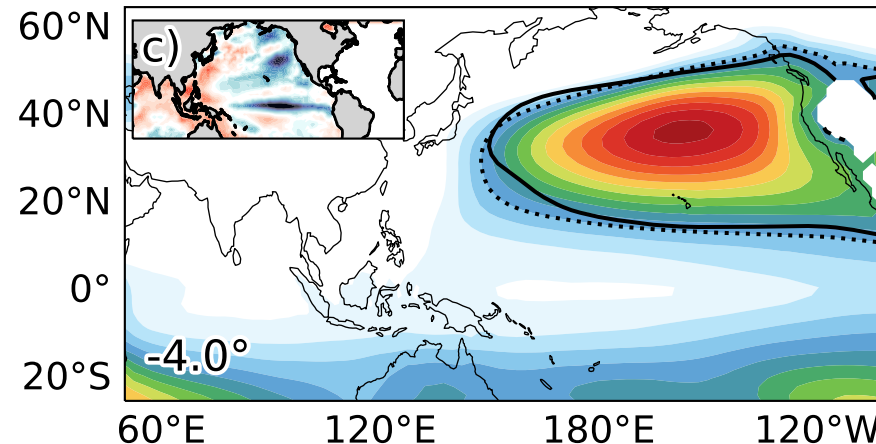
COMP2 4xWEST (global)



[m]



4xWEST minus ATL



4xWEST minus ATL+TIO

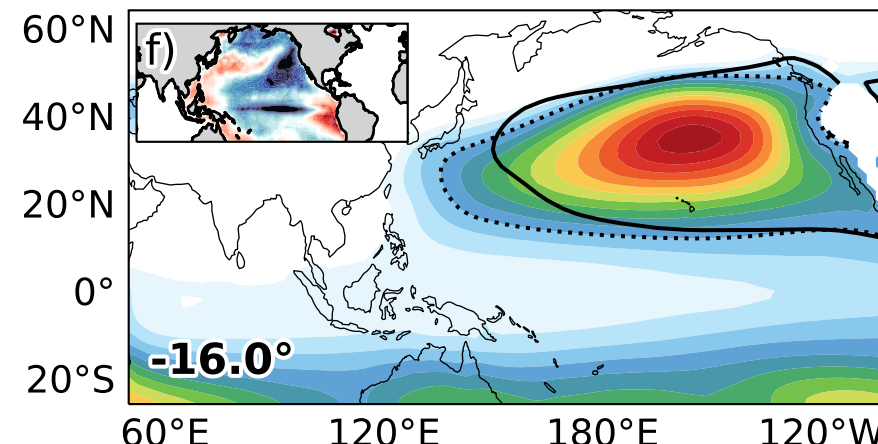
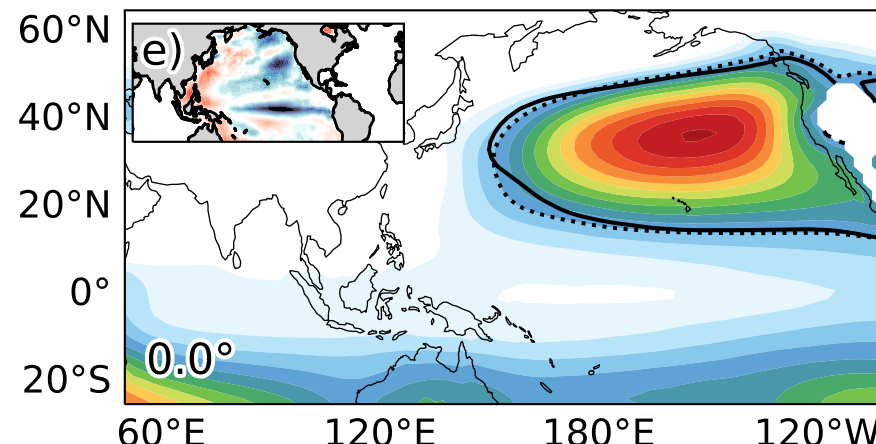


**Figure 5.**

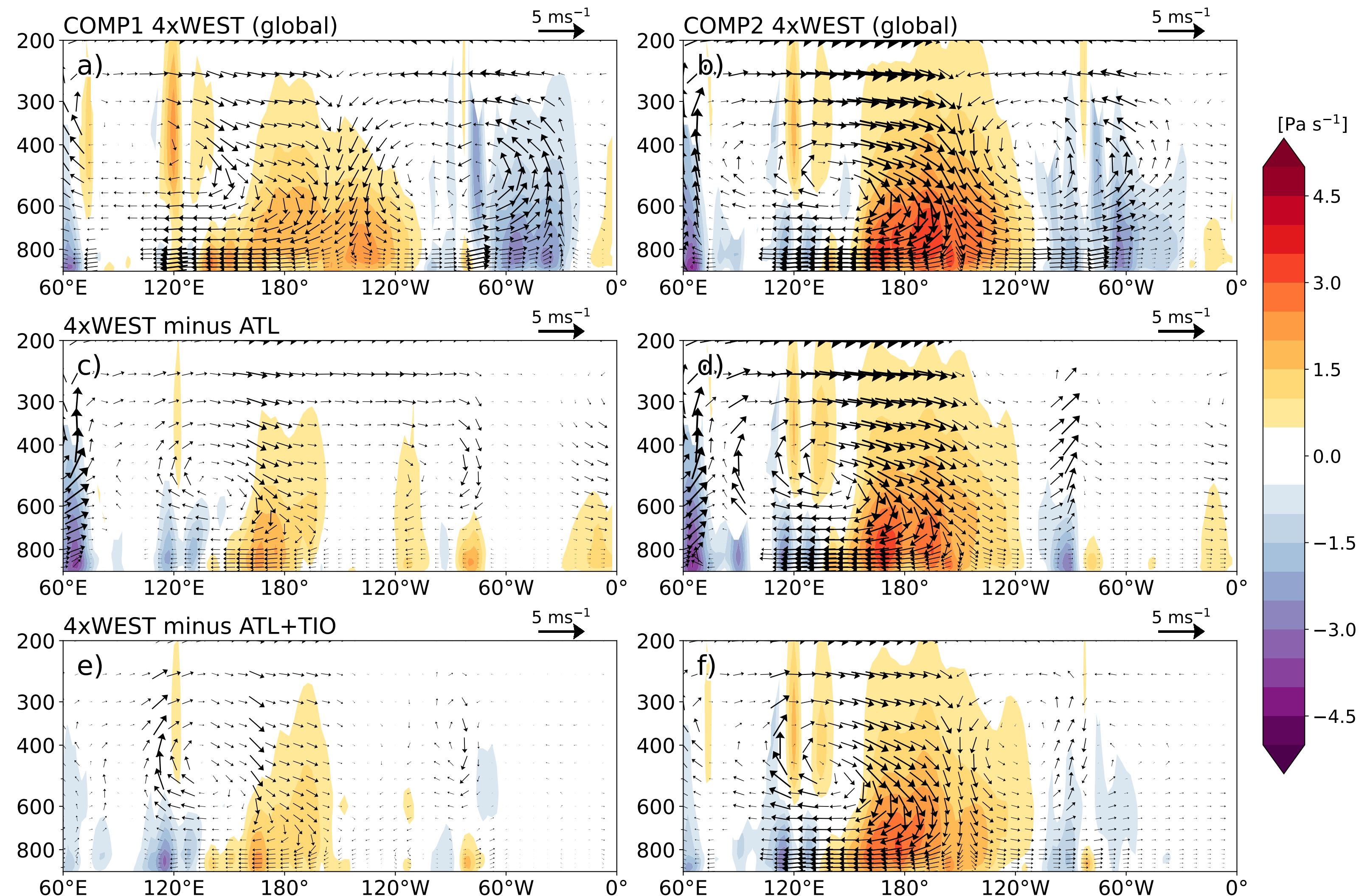


**Figure 6.**

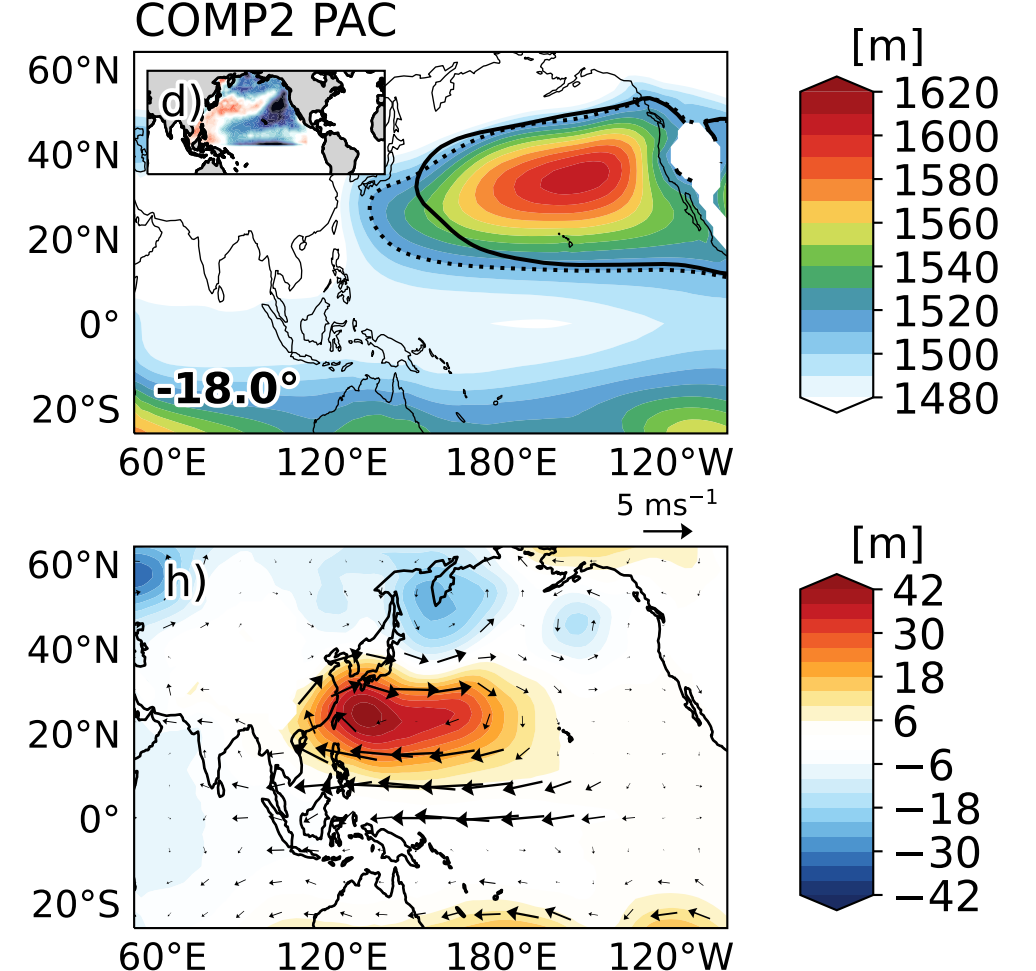
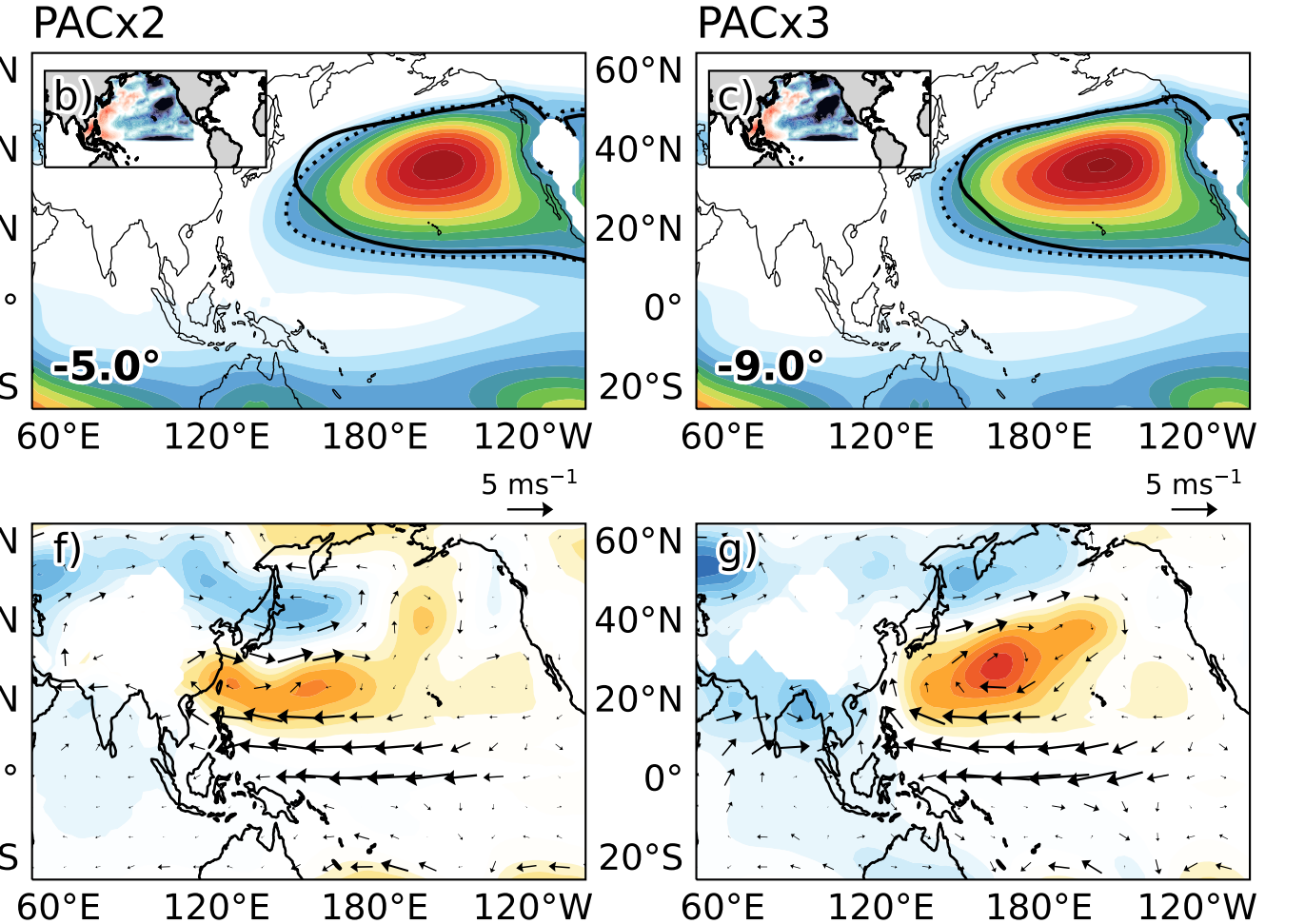
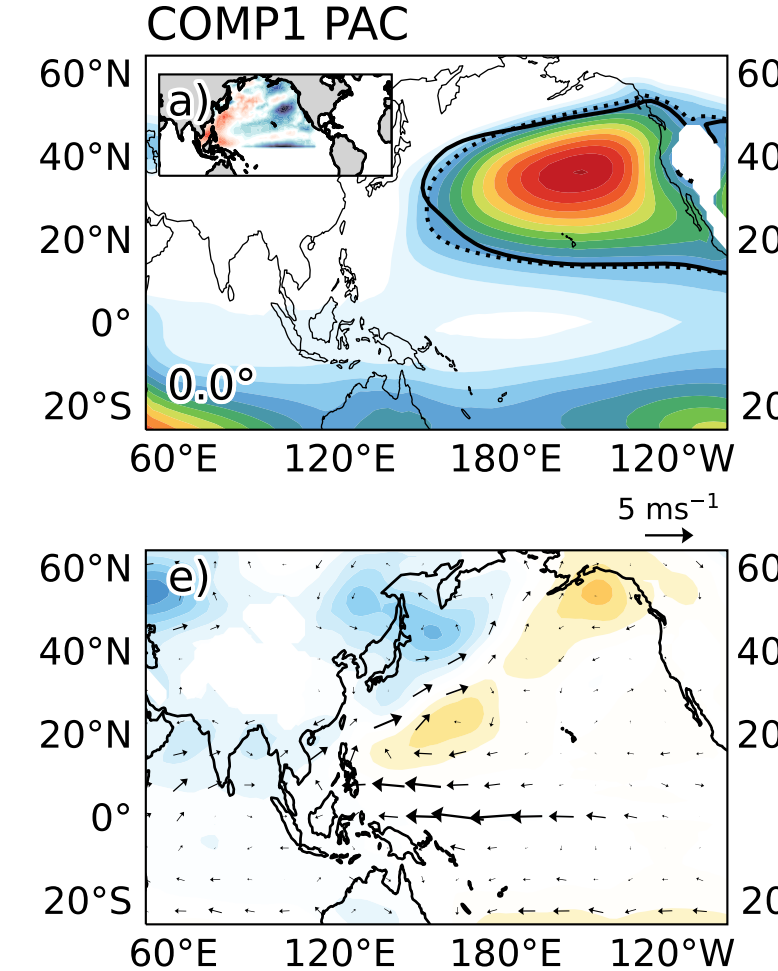
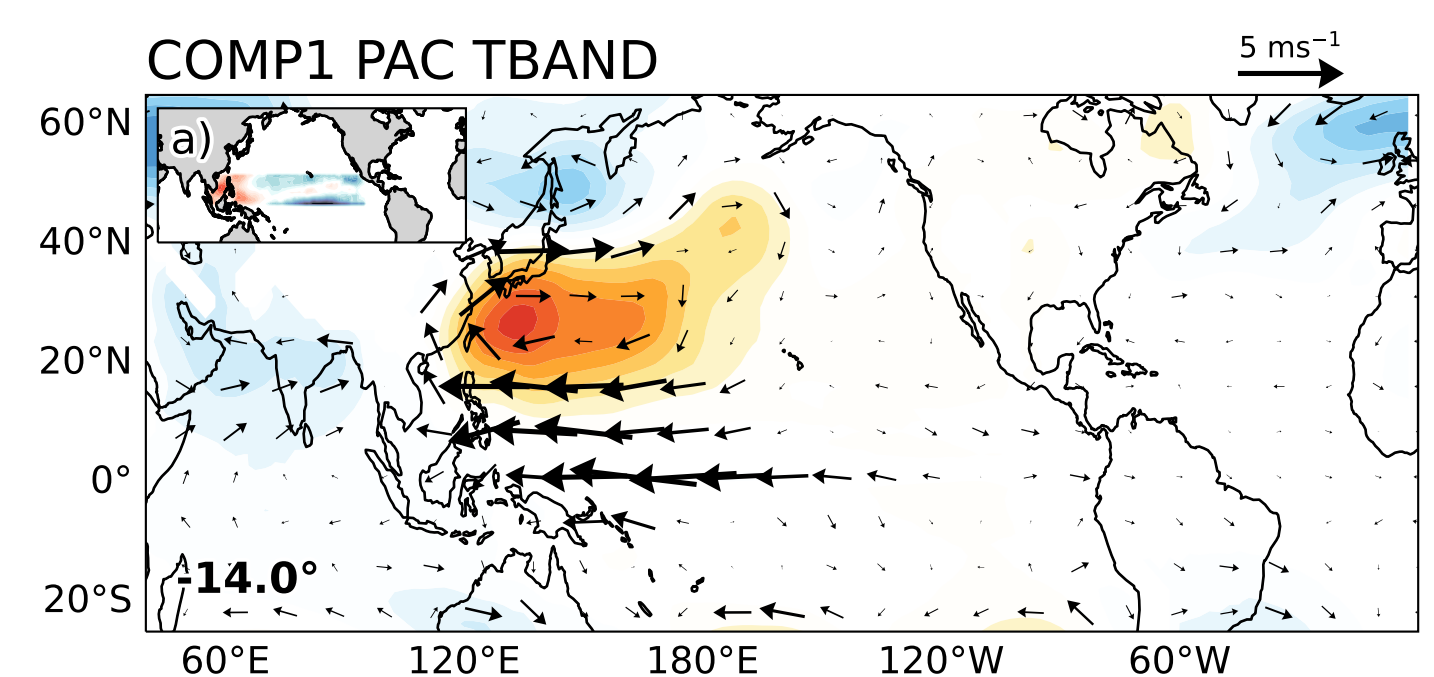
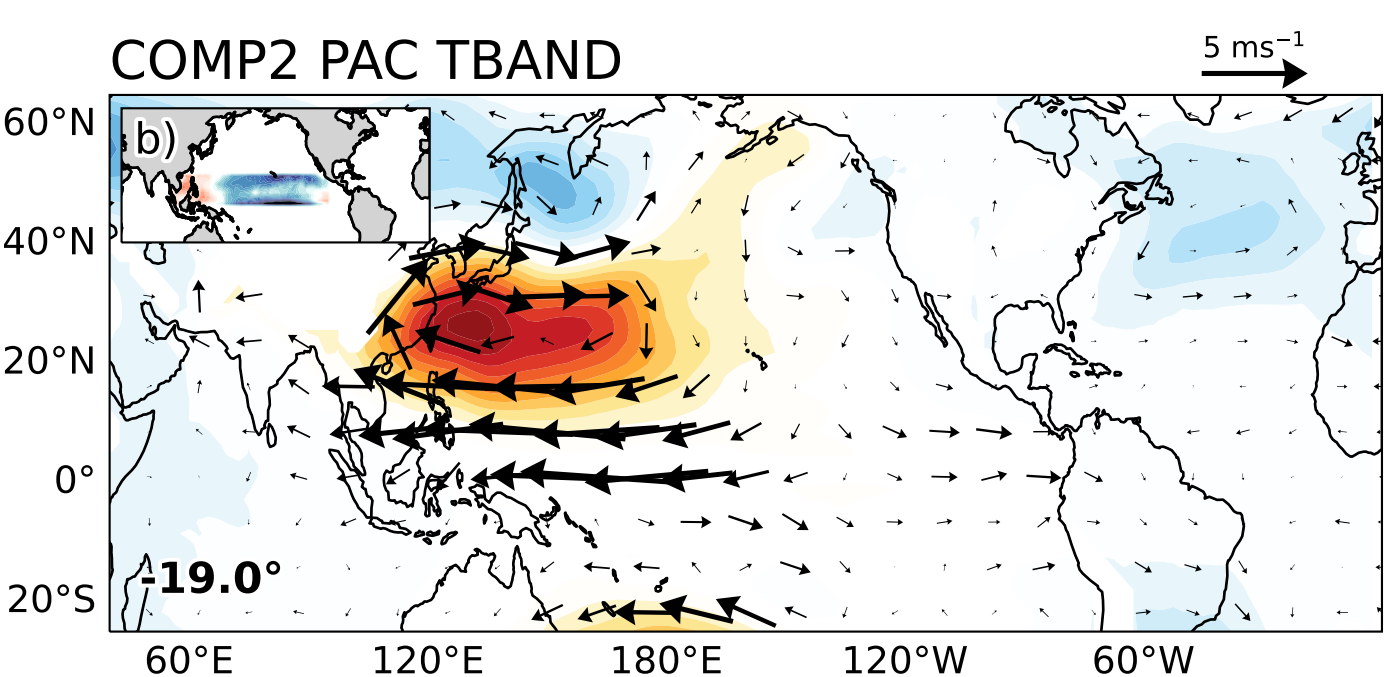


**Figure 7.**

COMP1 PAC TBAND



COMP2 PAC TBAND



PAC EXTBAND

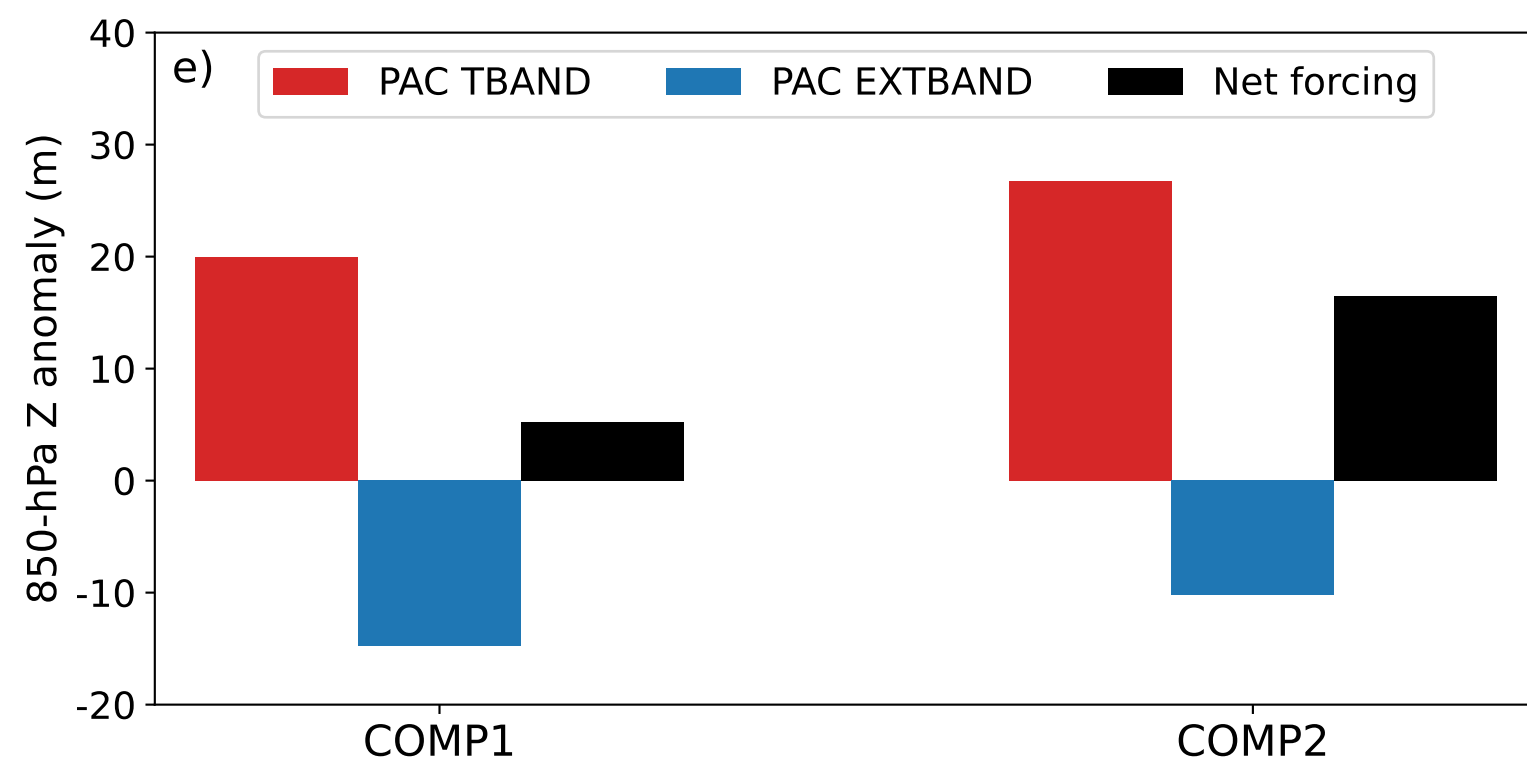
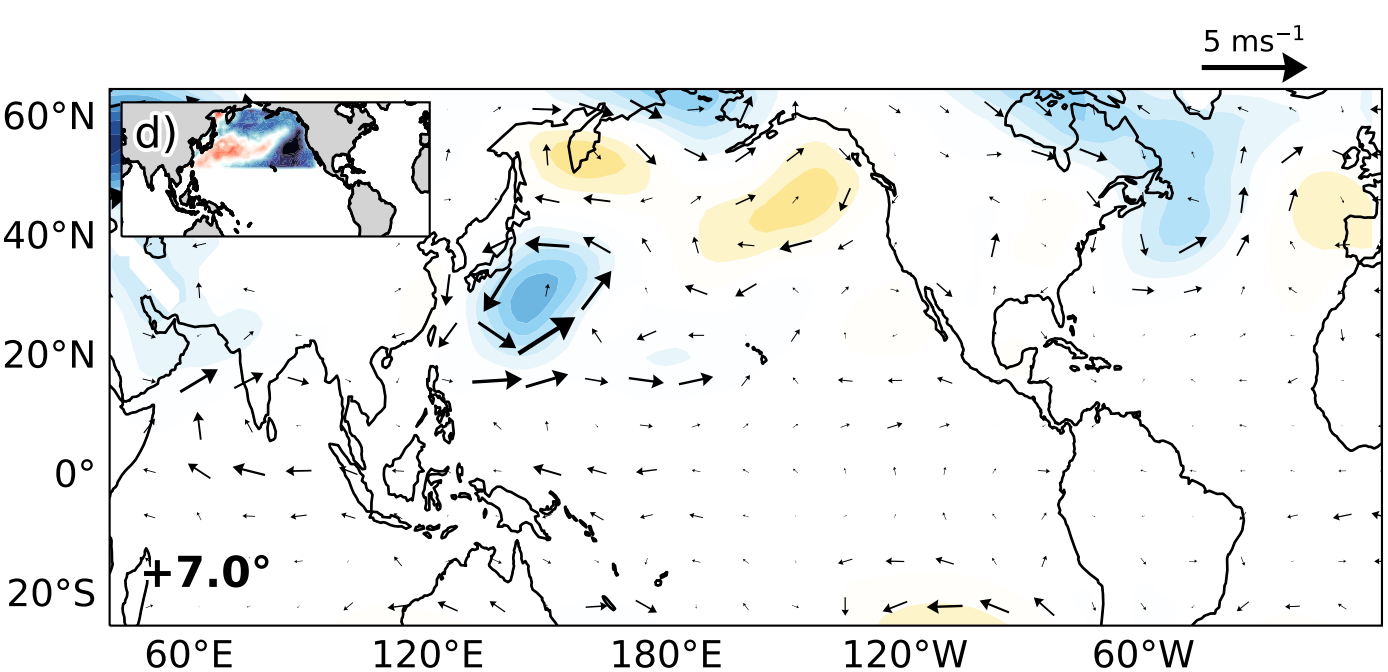
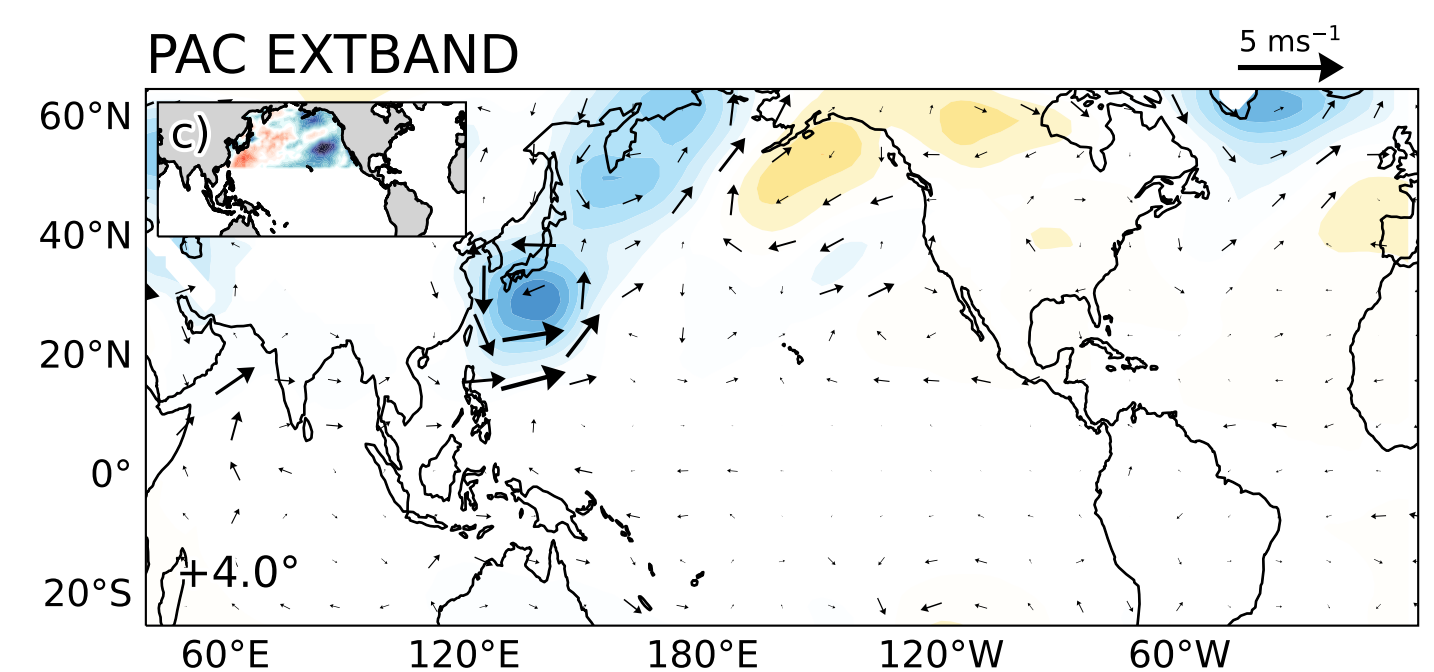
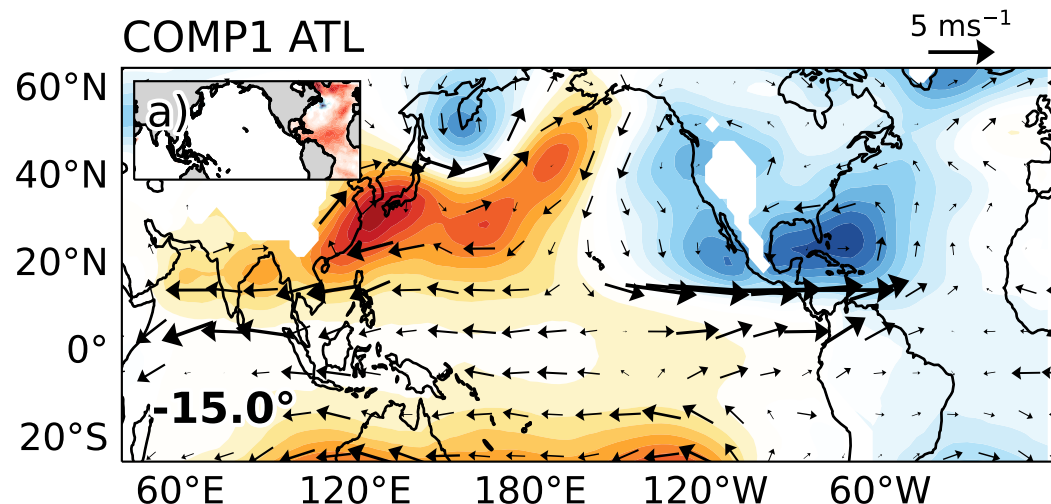
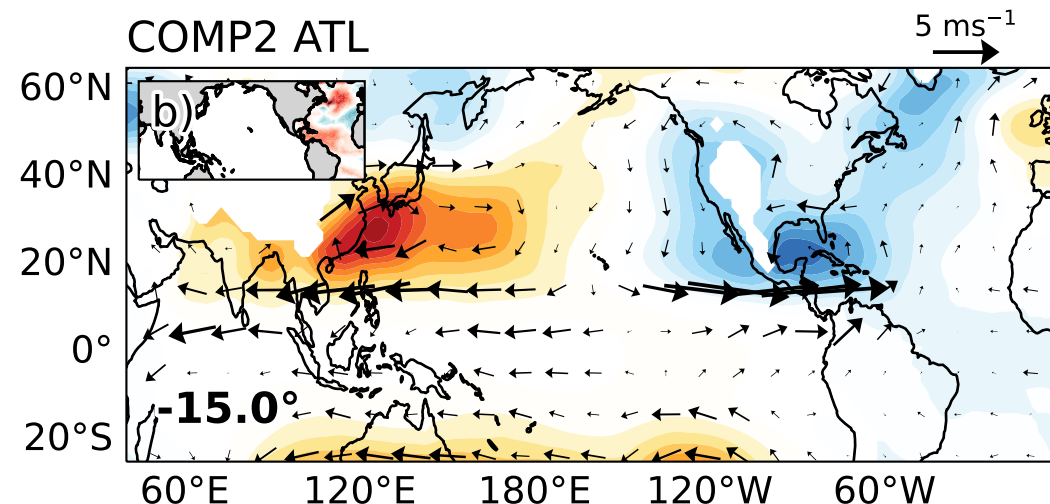


**Figure 8.**

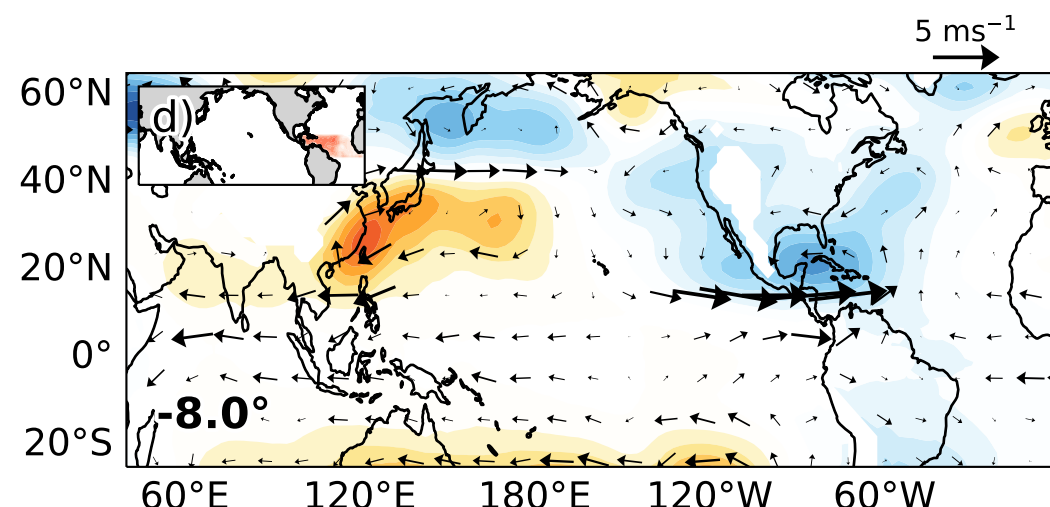
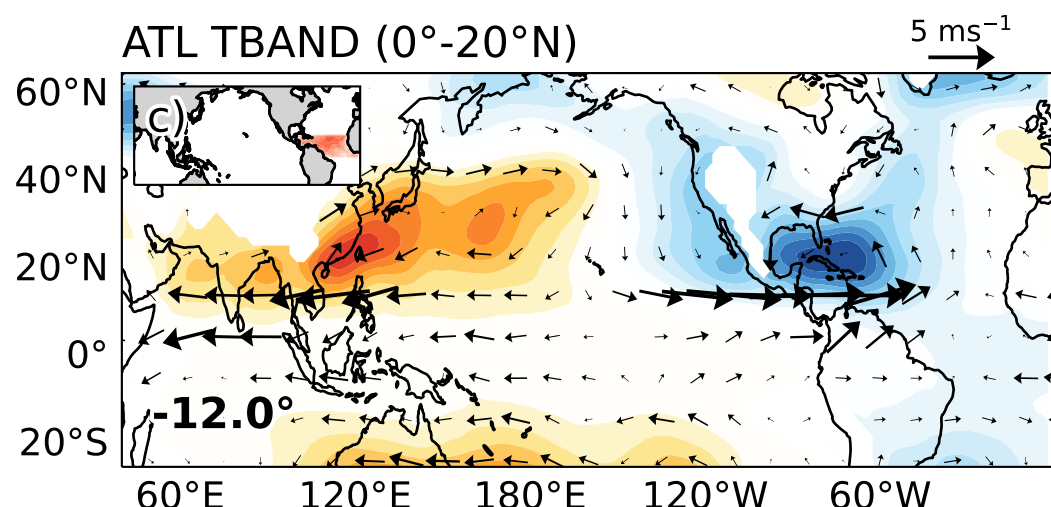
COMP1 ATL



COMP2 ATL



ATL TBAND (0°-20°N)



ATL EXTBAND (20°-60°N)

